On the stability of transient bimaterial contact in the presence of dry friction and slip

Gurrutxaga-Lerma, Beñat

DOI:
10.1016/j.ijsolstr.2023.112291

Document Version
Publisher's PDF, also known as Version of record

Citation for published version (Harvard):
Gurrutxaga-Lerma, B 2023, 'On the stability of transient bimaterial contact in the presence of dry friction and slip', *International Journal of Solids and Structures*, vol. 276, 112291.
https://doi.org/10.1016/j.ijsolstr.2023.112291

International Journal of Solids and Structures 276 (2023) 112291

Contents lists available at ScienceDirect

International Journal of Solids and Structures

journal homepage: www.elsevier.com/locate/ijsolstr

On the stability of transient bimaterial contact in the presence of dry friction and slip

Beñat Gurrutxaga-Lerma

School of Metallurgy and Materials, University of Birmingham, B15 2TT Edgbaston, Birmingham, UK

ARTICLE INFO

Keywords:
Elastodynamic
Contact
Plane strain
Stick
Slip
Friction

ABSTRACT

An analytic formulation for the study of planar elastodynamic contact in bimaterial interfaces subject to dry friction and slip is presented. Using the Wiener–Hopf technique, explicit analytical expressions for the elastic waves scattered by a planar contact interface are derived. Two cases are studied: (1) the uncoupled problem where it is assumed that normal and tangential loads cause, respectively, no tangential and vertical displacements; (2) the fully coupled problem, where they do. In both cases, an analytic formulation for determining the magnitude of the regions of stick and slip expected at the interface is offered. This provides a complete analytic account of the interfacial tractions and, as a results, serves to model the elastic wave scattering by contact interfaces, a problem of interest in fields as disparate as geophysics, non-destructive testing, and fracture mechanics. The uncoupled problem is shown to be inconsistent: the magnitude of the reciprocal displacements caused by the normal/tangential loads is non-negligible, and of the same magnitude as the interfacial slip distribution itself. The coupled problem is shown to lead to a matricial Wiener–Hopf problem the scattering kernel of which is non-commutative; an Abrahams approximation reliant on the Padé approximants is used to study the problem. It is shown that in many circumstances, the bimaterial contact interface is bound to detach locally, even when the far-field, steady-state solutions would predict otherwise. This is brought about by interfacial loading mismatches brought about by the coupling, and is shown to be affected by various factors: weak pressure loads, the friction coefficient, the disparity in the elastic constants of the media under contact. An useful analytic criteria for detachment is offered.

1. Introduction

This article concerns the study of the planar frictional contact conditions operating under time dependent (elastodynamic) loading across a flat interface involving two different elastic solids. Elastodynamic bimaterial contact, where an interface separating two different materials is subjected to time dependent loading or sliding, has received some attention in fracture mechanics (Cao and Evans, 1989; Liu et al., 1995; Rosakis et al., 1998), where the problem of a crack propagating across a bimaterial interface is crucial in understanding composite media delamination (Hutchinson and Jensen, 1990; Yang et al., 1991; Lambros and Rosakis, 1995; Golub and Doroshenko, 2019), film-to-substrate failure (Andrews and Kinloch, 1973; Cao and Evans, 1989; Leterrier, 2003; Stallard et al., 2006) and inclusion–matrix debonding in composite and crystalline materials (Mantič, 2009), particularly under impact bonding (Hassani-Gangaraj et al., 2019; Tiamiyu et al., 2022); and in other fields including non-destructive evaluation of internal flaws via elastic wave scattering techniques (Baik and Thompson, 1984; Delsanto and Scalerandi, 1998; Lavrentyev and Rokhlin, 1998; Jhang, 2009), the study of joints in biomechanical systems (Fregly et al., 2003; McKinley et al., 2006; Hériveaux et al., 2018), to study interfacial wear performance (Gurrutxaga-Lerma, 2019; Gurrutxaga-Lerma, 2020), and in geophysics, where often the fault surface separating dissimilar layers in shallow earth are neither perfectly welded nor perfectly lubricated (Rice, 1993; Weertman, 1980; Blanpied et al., 1995; Minato and Ghose, 2014; Kilgore et al., 2017).

In all these contexts, frictional contact arises as a result of the two surfaces coming into touch with one another under the action of time-dependent loads. The time dependent contact loads can be brought about by high speed, high strain rate remote loads (as could be the case for instance in the case of impact bonding (Hassani-Gangaraj et al., 2019) or in geophysics (Weertman, 1980)), by the relative sliding of the two surfaces at sufficiently high speeds (as could be the case in composite media delamination (Lambros and Rosakis, 1995)), or perhaps because the speed of sound in the relevant materials is sufficiently low

E-mail address: b.gurrutxagalerma.1@bham.ac.uk.

https://doi.org/10.1016/j.ijsolstr.2023.112291
Received 15 February 2022; Received in revised form 17 April 2023; Accepted 25 April 2023
Available online 13 May 2023

relative to the speed or rates at which the loads themselves are being applied (a situation commonly encountered in soft joints (McKinley et al., 2006)). In turn, the presence of a contact problem can be due to intrinsic reasons (i.e., due to the geometry or the configuration of the interface itself), or extrinsic reasons (i.e., brought about by the remote loading itself). This article is concerned with contact due to extrinsic causes: remote loads the effects of which propagate through the materials as elastic waves that are scattered by a contact interface. This is a typical concern in e.g. non-destructive testing and geophysics.

The possibility of intrinsic contact is non-trivial. Indeed, classical elasticity predicts a well-known logarithmic (oscillatory) stress singularity at the bimaterial mode I crack tip (Williams, 1959) that would imply interpenetration of the crack faces (Sinclair, 2004a,b; Broberg, 1999). Because said interpenetration is nonphysical, one of its classical remedies proposes substituting the interpenetration zone with a frictionless contact zone (Comminou, 1977; Comninou and Achenbach, 1978) which resolves the logarithmic oscillations. Alternative remedies have also managed to cure the oscillation, either by substituting linear elasticity for higher order deformation theories (Knowles and Sternberg, 1983; Geubelle and Knauss, 1994a,b,c; Gao and Shi, 1994), modifying the problem's topology through an intervening layer (Atkinson, 1974), or changing the geometry of the crack tip (Sinclair, 2004b; Broberg, 1999). With regards to elastodynamic accounts of bimaterial fracture, most theoretical work has focused on the asymptotics of crack tips and their energetics (e.g., Achenbach et al., 1976; Comninou and Achenbach, 1978; Rice, 1988; Yang et al., 1991; Liu et al., 1993; Yu and Yang, 1995; Huang et al., 1996), numerous numerical studies (e.g. Xu and Needleman, 1996; Needleman and Rosakis, 1999; Scala et al., 2017) of different aspects of bimaterial debonding and their experimental verification (e.g. Liu et al., 1993; Lambros and Rosakis, 1995; Liu et al., 1995).

Otherwise, under elastodynamic loading many situations arise where contact considerations become inevitable. For instance, in the presence of a normal compressive load, sliding mode II cracks inevitably entail a contact problem; this situation is typically encountered in geophysics, where sliding bimaterial interfaces are common sources of seismic events (Rice and Ruina, 1983; Blanpied et al., 1995), and has spanned remarkable research aimed at investigating the universality class of frictional laws beyond the local specificities of the contact problem (cf. Carlson and Langer, 1989; Olami et al., 1992; Rice, 1993; Scholz, 1998; Lapusta et al., 2000; Scholz, 2019). Likewise, contact considerations become critical when studying bimaterial mode I cracks propagating at transonic speeds. This is because the normal interfacial tractions, which under quasi-static loading tend to be tensile, may reverse their sign in the transonic regime (Xu and Needleman, 1996; Needleman and Rosakis, 1999; Hao et al., 2004), a fact that suggests of the presence of an extended contact zone along the crack faces. Experimental and modelling evidence of the importance of the contact zone in elastodynamic fracture has since compounded, particularly when studying transonic crack propagation (Hao et al., 2004).

Despite the inherent theoretical difficulties involved in offering a complete treatment of elastodynamic contact similar to the one existing for static loading (see Johnson, 1987; Barber, 2018), various studies of elastodynamic contact exist. An important branch of these accounts focus on the presence of dynamic singularities at specific moving speeds, namely the speeds of sound (Craggs and Roberts, 1967; Brock, 2002) and the Rayleigh wave speed (Georgiadis and Barber, 1993; Brock, 2012): when two rubbing surfaces come together and experience a relative motion (e.g., a sliding indenter) the speed of which approaches either the speeds of sound or the Rayleigh wave speed, studies typically performed in the steady state and under frictionless conditions predict the presence of elastic singularities the energetics of which would bar contact in the trans and supersonic regimes (Craggs and Roberts, 1967; Georgiadis and Barber, 1993; Slepyan and Brun, 2012). Likewise, the stability of frictional sliding can be brought into question over similar considerations (Comninou and Dundurs, 1977; Comninou, 1984; Adams, 1995): as is the case with high speed crystalline dislocations (Gurrutxaga-Lerma et al., 2020), transonic sliding at the interface would *prima facie* appear impossible on account of the system's elastic energy diverging at said speeds (Eshelby, 1956; Freund, 1972); this would make overcoming the sound barriers impossible, and make transonic motion dissipative unless further considerations are made. For instance, recently Slepyan and Brun (2012) have shown that in frictionless indenters transonic motion is possible provided one accepts that the material can absorb excess energy via inelastic deformation. Frictional elastodynamic sliding, in turn, has been shown to be ill-posed (Simoes and Martins, 1998) when the frictional law is Coulombian, and several alternative frictional laws able to regularise the problem have been proposed (Rice et al., 2001; Abedi and Haber, 2014). Using ray analysis, it is possible to study the presence of regions of stick and slip at frictional elastodynamic interfaces under cyclic and plane waves. Chez and coworkers (Chez et al., 1978) used the approach to study the width of the regions of stick in bimaterial interfaces subjected to planar waves using a corrective solution approach analogous to that employed in the classical Cattaneo–Mindlin problem in elastostatic frictional contact (Cattaneo, 1938; Barber, 2018); likewise numerical approaches based on similar considerations have been proposed with which to model elastodynamic frictional contact (e.g.,(Abascal, 1995; Blanloeuil et al., 2014, 2019)). In both cases, adhesion, slip, and separation is reported at different loading rates and for different frictional coefficients (Comninou, 1984), usually focused on unimaterial interfaces, for which the presence of regions of separation in frictional contacts subject to plane strain loads have been reported (Comninou and Dundurs, 1977).

Generally speaking, it appears that if the incident elastic shear waves reaching a frictional interface are sufficiently large, or the contact pressure sufficiently weak, conditions may arise that prompt the interface to slip (Chez et al., 1978) or detach (Comninou and Dundurs, 1977; Yu et al., 2006) even if the remote loading ought to lead to stable contact once the transient has subsided. The exact way waves of detachment and/or slip may form is unclear, particularly if the interface appears in a bimaterial medium. Further, a fully transient treatment of this problem appears to be unavailable. The non-linear nature of the problem only complicates matters further: slip arises to ensure Coulomb's law is not violated, and detachment if the contact pressure becomes tensile; neither condition can be known a priori without evaluating the transient loads involved at the interface.

This article derives a fully transient, analytic formulation with which to study the elastodynamic bimaterial contact via the corrective solution approach commonly encountered in elastostatics (Dini and Hills, 2003; Hills et al., 1996; Nowell et al., 1988; Barber, 2018). Its aims are dual. On the one hand, this article seeks to offer a complete analytic treatment of the interfacial tractions involved in dry frictional contact. As has been argued above, the interest of these expressions extends beyond this specific problem to other bimaterial interface problems including fracture mechanics, wave diffraction at material faults of interest in delamination, non-destructive testing, and seismology, and can be also employed in alternative geometries or other problems concerning elastodynamic bimaterial systems. On the other hand, this article seeks to determine the local stability of the transient contact problem when driven by loads, and the mathematical considerations necessary to model said stability and the possibility of local detachment.

In the approach used in this article, slip is presented as a consequence of the need to establish the force balance at the interface and obey Amonton's law of friction (see Barber, 2018). The article is structured as follows: In Section 2 the mathematical problem under consideration is outlined: it presents a planar, quiescent (non-sliding) interface between two elastically dissimilar bodies subject to remote transient loads. Contact is maintained by a remote pressure load, and shear is transferred across the interface by means of Coulomb-type dry friction. In Section 3 the analytic expression for the interfacial tractions

induced by this remote loading are derived by means of the Wiener–Hopf technique (Noble, 1958). This leads to the analytic expression of the transient 'corrective' traction (see Dini and Hills, 2004; Hills et al., 1996) in a bimaterial interface; this corrective traction models the shear traction that would be induced by an arbitrary distribution of slip acting at the interface. This slip is necessary to ensure that the local force balance at the interface: if the frictional force binds together normal and shear tractions, then the interface can only accommodate their mismatch by slipping. In Section 4, the uncoupled problem resulting from the common assumption that normal loads induce no interfacial shear load (and vice versa, cf. Barber, 2018, ch.9) is studied. Section 4 also shows that the bimaterial interface cannot exist in a state of uncoupled contact without violating its own self-consistency. This situation does not arise in single material contacts because of the symmetry of the elastodynamic Green's function (Gurrutxaga-Lerma, 2020); however, when the interface divides two elastically dissimilar bodies, this article shows that the interface becomes vertically incompatible (i.e., interpenetrating or separating) unless the fully coupled problem is considered. To that end, Section 5 introduces an analytic formulation with which to solve the fully coupled contact problem; the non-commutativity of the resulting Wiener–Hopf problem is discussed, and a recursive solution based on the Abrahams decomposition (Abrahams, 1996) of the Riemann–Hilbert scattering kernel is introduced. This enables the correction of the interfacial force balance and regain self-consistency at the interface. However, as is discussed in Section 6, the ensuing contact problem can easily become unstable. This is shown to occur when the interfacial normal load becomes positive, in which case contact is lost, and the interface detaches. A criterion for detachment is derived, and examined under varied loading and material conditions. The article closes in Section 7, where it concluded that bimaterial contact can be stable, but that if the elastic constants of the materials in contact are sufficiently dissimilar, friction is weak, or the remote loading weak relative to the applied shear loads, the interface is likely to detach.

2. Statement of the problem

We consider two planar, elastic half-spaces be in contact along an infinite interface as depicted in Fig. 1. Both solids are linear elastic but *dissimilar* from one another: material 1 has shear modulus μ_1, Lamé parameter λ_1, and density ρ_1; conversely material 2 has elastic constants μ_2, λ_2, and ρ_2. The corresponding speeds of sounds are labelled as $c_t^{(n)} = \sqrt{\mu_n/\rho_n}$, $c_l^{(n)} = \sqrt{(\lambda_n + 2\mu_n)/\rho_n}$, $n = 1, 2$; for convenience throughout this work will also employ the slownesses of sound $a_n = 1/c_l^{(n)}$ and $b_n = 1/c_t^{(n)}$.

As is indicated in Fig. 1, the system is subjected to two remote time-dependent symmetric distributed loads, a normal load $P(t)$ and a shear load $Q(t)$. We assume that both loads act solely for $t > 0$, and that the system is unloaded and at rest for $t < 0$. Under the action of these two loads, two sets of elastic waves travelling at different speeds are launched across each medium, reaching the interface at different instants in time. On their own, the two half spaces are unstuck, and would be free to slide relative to one another were not for the action of the remote normal force $P(t)$, that establishes the contact. We assume that contact exists for $x > 0$, and that for $x < 0$ the interfaces remain free. This is done to be able to model the edge of a contact zone without having to account for rarefaction waves incoming from other free surfaces where one or the two materials to be shaped like a generalised wedge. Contact alone suffices for normal loads to be transferred across the interface, so that the first contact condition be that the interfacial normal traction $p(x,t) = -\sigma_{yy}(x,t)$ on either material be the same:

$$p_1(x,t) = p_2(x,t) \equiv p(x,t) \tag{2.1}$$

Naturally, $p(x,t)$ ought to be compressive for contact to exist. Hereafter, we adopt the convention that $p(x,t) > 0$ denotes compression at the interface and that, accordingly, $\sigma_{yy} < 0$ denotes compression.

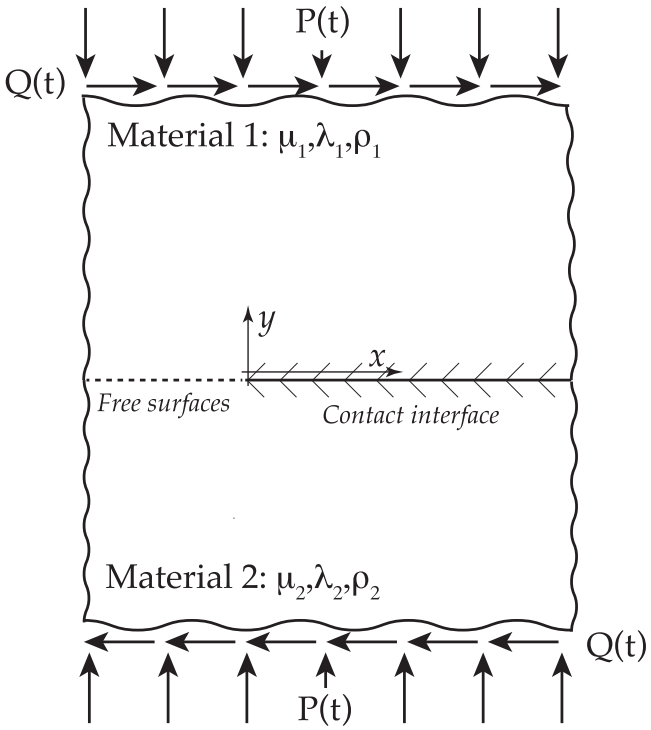

Fig. 1. Diagram of the problem under consideration: two elastic half-spaces under plane strain conditions, in frictional contact over $x \in \mathbb{R}^+$, subjected to symmetric remote distributed loading $P(t)$ and $Q(t)$, and with shear moduli μ_1, μ_2, Lamé parameters λ_1, λ_2, and densities ρ_1 and ρ_2, and friction coefficient f.

Under the action of the remote shear loads $Q(t)$, a further interfacial shear traction $q(x,t) \equiv \sigma_{xy}(x,t)$ will be present at the interface. In the problem under consideration here, the interface can only transfer shear loads via a dry frictional load, which obeys Coulomb's law, namely

$$q(x,t) \leq f\,\mathrm{sign}(f)p(x,t) \tag{2.2}$$

where by $\leq$ we imply that the interfacial shear traction can be less that or up to the frictional traction, f is the dry friction coefficient (assumed to be the same for static and dynamic contact), and $\mathrm{sign}(f)$ is defined so that the sign of the shear traction opposes the relative motion of the two bodies in contact at the interface. Because here $p(x,t) > 0$ denotes compression, for $q(x,t)$ to oppose the relative motion at the interface the $\mathrm{sign}(f)$ is defined so that

$$\mathrm{sign}(f) = \frac{[\![\dot{u}_x]\!]}{|[\![\dot{u}_x]\!]|} \tag{2.3}$$

where $[\![\dot{u}_x]\!] = \dot{u}_x^{(1)} - \dot{u}_x^{(2)}\big|_{\text{interface}}$ is the relative tangential velocity at the interface, with $[\![u_x]\!] = u_x^{(1)} - u_x^{(2)}$ the relative displacement or tangential displacement in it. Note that Eq. (2.2) is valid on either side of the interface. If $q(x,t)$ and $p(x,t)$ are both caused by remote loading, there is no reason to assume that the inequality Eq. (2.2) will be maintained across the whole interface. This leads to distinguishing two distinct regions of contact:

(1) The region over which $q(x,t) < f\,\mathrm{sign}(f)p(x,t)$ will be a region of *stick*. The material points will be adhered.
(2) The region over which $q(x,t)$ would exceed the magnitude of the frictional traction, $f\,\mathrm{sign}(f)p(x,t)$ will be a region of *slip*. To avoid violating Coulomb's law, the interfacial points are forced to slip relative to one another, i.e., experience a relative displacement $[\![u_x]\!] = u_x^{(1)} - u_x^{(2)} \equiv u(x,t)$. This relative slip displacement at the interface prompts an additional interfacial shear stress $q^{\text{slip}}(x,t) \equiv s(x,t)$, such that $q(x,t) + s(x,t) = f\,\mathrm{sign}(f)p(x,t)$ restores interfacial equilibrium and Coulomb's law.

Thus, in the present work we seek to find:

(1) The interfacial tractions $p(x,t)$ and $q(x,t)$ due to a remote normal and shear loads, respectively.
(2) The interfacial traction $s(x,t)$ due to a distribution of slip acting at the interface.

With these in place, we ought to be able to study the equilibrium conditions at the interface, namely when

$$q^{\text{tot}}(x,t) = f\,\text{sign}(f)p^{\text{tot}}(x,t) = f\,\text{sign}(f)p^{\text{tot}}(x,t) \tag{2.4}$$

where the superindex 'tot' denotes the total traction acting at the interface, whether it be caused by remote loading, by a distribution of slip, or both.

3. The interfacial tractions in an uncoupled interface

We begin by giving the expressions for the interfacial tractions that would be involved in an uncoupled problem. By uncoupled problem, we mean the notional situation where the remote normal and tangential loads do not cause, respectively, a shear and normal tractions at the contact interface or that these can be neglected. This would serve to model an interface where remote normal and tangential loads do not produce, respectively, a horizontal and a vertical displacement at the interface. In unimaterial situations, uncoupled contact is a reasonable approximation (Barber, 2018; Gurrutxaga-Lerma, 2019; Gurrutxaga-Lerma, 2020) owing to the material symmetry across the interface. Obtaining the interfacial tractions for the uncoupled problem is the first step to determine whether said situation is possible in the bimaterial case; as we detail in Section 4.2, it turns out to be an unacceptable approximation: the reciprocal displacements entailed by the interfacial tractions are as large as the uncoupled ones, so the uncoupled assumption loses its own internal consistency. The tractions given in this section are nevertheless not without merit, as they are still necessary for the fully coupled problem discussed in Section 5.

Thus, we require the analytical expressions for the following terms:

(1) The interfacial normal traction $p(x,t)$ due to a mode I crack along a bimaterial interface.
(2) The interfacial shear traction $q(x,t)$ due to a mode II crack along bimaterial interface.
(3) The interfacial shear traction $s(x,t)$ due to an arbitrary $[u_x] = \phi(x,t)$ slip distribution along a bimaterial interface.

We discuss each of these terms in the sequel. In all cases, the notional crack has its tip at $x = 0$.

3.1. Normal and tangential interfacial tractions in the uncoupled problem

These tractions were obtained by the author in Gurrutxaga-Lerma (2020) for suddenly applied 'shock' loads $P(x,t) = P_0 H(t)$ and $Q(x,t) = Q_0 H(t)$. The remote normal load P entails an interfacial normal traction $p(x,t)$, and the remote shear traction Q an interfacial shear traction $q(x,t)$. The interface (and therefore the support of the tractions) is given for $x > 0$, along the nominal contact interface. The two tractions are given by:

$$p(x,t) \equiv p_+(u) = -\frac{1}{\pi}\int_{a_1}^{u} \text{Im}\left[P_+\left(-u'\right)\right] \mathrm{d}u' \tag{3.1}$$

$$q(x,t) \equiv q_+(u) = -\frac{1}{\pi}\int_{a_1}^{u} \text{Im}\left[Q_+\left(-u'\right)\right] \mathrm{d}u' \tag{3.2}$$

where

$$P_+(k) = \frac{P_0}{k}\left[\frac{K_+(0)}{K_+(k)} - 1\right] \tag{3.3}$$

and

$$Q_+(k) = \frac{Q_0}{k}\left[\frac{G_+(0)}{G_+(k)} - 1\right] \tag{3.4}$$

The derivation of the kernels $K_+(k)$ and $G_+(k)$ is detailed in Gurrutxaga-Lerma (2020). The results are quoted in Appendix A. We note that if the remote applied loads were to take the more general mathematical form $P(x,t) = P(t)$ and $Q(x,t) = Q(t)$, then the interfacial normal and shear tractions (say, $p_g(x,t)$ and $q_g(x,t)$) would be given by the convolution integrals:

$$p_g(x,t) = \int_0^{\infty} \frac{\partial p(x,t-t')}{\partial t}\frac{P(t')}{P_0}\mathrm{d}t', \tag{3.5}$$

$$q_g(x,t) = \int_0^{\infty} \frac{\partial q(x,t-t')}{\partial t}\frac{Q(t')}{Q_0}\mathrm{d}t' \tag{3.6}$$

where $p(x,t-t')$ and $q(x,t-t')$ are obtained from Eqs. (3.1) and (3.2) respectively.

3.2. Tangential traction due to a distribution of interfacial slip

We now seek the tangential traction due to an arbitrary horizontal distribution of slip. We shall employ the following strategy. First, we will solve the problem of a pulse displacement jump $[\![u_x(x,y=0,t)]\!] = \delta(x-x_0)\delta(t-t_0)$ acting on the interface between the two dissimilar materials. The interface is the positive axis of abscissae, $x > 0$, whilst the negative axes describes two free surfaces, for $y > 0$ (material 1) and $y < 0$ (material 2). Owing to the linearity of the governing equation (see Eq. (3.7)), the resulting interfacial shear traction $s_+(x,t)$ can then be used via convolution to express the interfacial shear traction due to a general distribution of slip; this second step is detailed in Section 3.2.2.

Each of the materials is governed by the Navier–Lamé equation:

$$(\lambda_n + \mu_n)u^{(n)}_{j,ji} + \mu_n u^{(n)}_{i,jj} = \rho_n \ddot{u}^{(n)}_i \tag{3.7}$$

where repeated index denotes summation, and $n = 1,2$ denotes the first ($y > 0$) or the second ($y < 0$) material. The problem under consideration is in plane strain, whereupon the Navier–Lamé equation can be divided into two separate monochromatic wave equations by means of the scalar Kelvin–Helmholtz potentials ψ_n and ϕ_n (cf. Eringen and Suhubi, 1975). The potentials are such that

$$u^{(n)}_x = \frac{\partial \phi_n}{\partial x} + \frac{\partial \psi_n}{\partial y}, \qquad u^{(n)}_y = \frac{\partial \phi_n}{\partial y} - \frac{\partial \psi_n}{\partial x} \tag{3.8}$$

Upon substituting Eq. (3.8) on Eq. (3.7) we obtain the two governing equations of the problem:

$$\frac{\partial^2 \phi_n}{\partial x^2} + \frac{\partial^2 \phi_n}{\partial y^2} = a_n^2 \frac{\partial^2 \phi_n}{\partial t^2} \tag{3.9}$$

$$\frac{\partial^2 \psi_n}{\partial x^2} + \frac{\partial^2 \psi_n}{\partial y^2} = b_n^2 \frac{\partial^2 \psi_n}{\partial t^2} \tag{3.10}$$

where

$$a_n = \frac{1}{c_l^{(n)}} = \sqrt{\frac{\rho_n}{\lambda_n + 2\mu_n}}, \qquad b_n = \frac{1}{c_s^{(n)}} = \sqrt{\frac{\rho_n}{\mu_n}} \tag{3.11}$$

are the longitudinal and the transverse slownesses of sound, respectively, in the material n. Similarly $c_l^{(n)}$ and $c_t^{(n)}$ are the longitudinal and transverse speeds of sound, respectively.

The boundary conditions relevant for the interfacial displacement are the following:

$$\sigma^{(n)}_{yy}(x,0,t) = 0 \qquad x \in \mathbb{R} \tag{3.12}$$

$$\sigma^{(n)}_{xy}(x,0,t) = 0 \qquad x \in \mathbb{R}^- \tag{3.13}$$

$$[\![u_x(x,0,t)]\!] \equiv u^{(1)}_x(x,0,t) - u^{(2)}_x(x,0,t) \tag{3.14}$$

$$= \delta(x-x_0)\delta(t-t_0) \qquad x \in \mathbb{R}^+ \tag{3.15}$$

where here we use $[\![u_x]\!] = u^{(1)}_x(x,0,t) - u^{(2)}_x(x,0,t)$to denote the discontinuity in horizontal displacement across the interface. We also require continuity of all stress components across the contact interface.

The solution we achieve in the sequel relies on the Wiener–Hopf technique (Noble, 1958). We wish to use integral transform methods

which invariably apply over the whole real line. However, the boundary conditions in Eq. (3.15) apply on different segments of the real line. Therefore, it is necessary to extend by continuity the boundary conditions in Eq. (3.15) to the whole real line. This is achieved by introducing two unknown functions, $s_+(x,t)$ and $u_-(x,t)$, with finite support on $x \in \mathbb{R}^+$ and $x \in \mathbb{R}^-$ respectively, and such that

$$\sigma_{yy}^{(n)}(x,0,t) = 0, \qquad x \in \mathbb{R} \tag{3.16}$$

$$\sigma_{xy}^{(n)}(x,0,t) = s_+(x,t), \qquad x \in \mathbb{R} \tag{3.17}$$

$$[\![u_x(x,0,t)]\!] \equiv u_x^{(1)}(x,0,t) - u_x^{(2)}(x,0,t) = \\ = \delta(x-x_0)\delta(t-t_0) + u_-(x,t), \qquad x \in \mathbb{R} \tag{3.18}$$

We note that $s_+(x,t)$ is the slip distribution we seek, and $u_-(x,t)$ the jump in the horizontal u_x displacement component across the free surfaces.

In order to solve the problem, we introduce the following Laplace transforms:

$$\hat{f}(x,y,s) = \int_0^\infty f(x,y,t)e^{-st}\mathrm{d}t, \\ F(k,y,s) = \int_{-\infty}^\infty \hat{f}(x,y,s)e^{-ksx}\mathrm{d}x \tag{3.19}$$

We note that, therefore, all capitalised variables are used to denote the dual Laplace transform of the non-capitalised ones. E.g., the Laplace transform of the stress component σ_{ij} will be denoted by Σ_{ij}, and that of the Kelvin potentials ϕ and ψ by Φ and Ψ, respectively.

Using these Laplace transforms, we can reduce the boundary conditions to a single Wiener–Hopf equation:

$$\mu_n\left[(b_n^2-2a_n^2)s^2\Phi_n + 2\frac{\partial^2\Phi_n}{\partial y^2} - 2sk\frac{\partial\Psi_n}{\partial y}\right]_{y=0} = 0 \\ \mu_n\left[2sk\frac{\partial\Phi_n}{\partial y} + \frac{\partial^2\Psi_n}{\partial y^2} - s^2k^2\Psi_n\right]_{y=0} = \frac{S_+(k)}{s^2} \\ \left[\left(\frac{\partial\Psi_1}{\partial y} + sk\Phi_1\right) - \left(\frac{\partial\Psi_2}{\partial y} + sk\Phi_2\right)\right]_{y=0} = \\ = e^{-s(t_0+kx_0)} + \frac{U_-(k)}{s^3} \tag{3.20}$$

where we have defined

$$S_+(k;s) = s^2\int_{-\infty}^\infty \hat{s}_+(x,y,s)e^{-skx}\mathrm{d}x, \\ U_-(k;s) = s^3\int_{-\infty}^\infty \hat{u}_-(x,y,s)e^{-skx}\mathrm{d}x \tag{3.21}$$

The governing Eq. (3.10) transform into

$$\frac{\partial^2\Phi_n}{\partial y^2} = \alpha_n(k)s^2\Phi_n, \qquad \frac{\partial^2\Psi_n}{\partial y^2} = \beta_n(k)s^2\Psi_n \tag{3.22}$$

where $\alpha_n(k) = \sqrt{a_n^2-k^2}$, $\beta_n(k) = \sqrt{b_n^2-k^2}$.

The solutions to the governing equations can be written to take the form:

$$\Phi_1(k,y,s) = C_{\phi1}(s,k)e^{-s\alpha_1(k)y}, \qquad (y>0) \\ \Psi_1(k,y,s) = C_{\psi1}(s,k)e^{-s\beta_1(k)y} \qquad (y>0) \\ \Phi_2(k,y,s) = C_{\phi2}(s,k)e^{s\alpha_2(k)y}, \qquad (y>0) \\ \Psi_2(k,y,s) = C_{\psi2}(s,k)e^{s\beta_2(k)y}, \qquad (y<0) \tag{3.23}$$

where $C_{\phi n}$ and $C_{\psi n}$ are integration constants. Thus, we are faced with a problem consisting of 6 unknowns (the four integration constants and $P_+(k)$ and $U_-(k)$), for which we have in principle only 5 equations. This will allow us to reduce the problem to one of Wiener–Hopf type, by adequate manipulation of the continuity requirements across the interface. In particular, the stress field across the interface for $y=0$ must be continuous, which means that

$$\Sigma_{yy}\Big|_{y=0} = \mu_1\left[(b_1^2-2k^2)s^2C_{\phi1} + 2s^2\beta_1kC_{\psi1}\right] \\ = \mu_2\left[(b_2^2-2k^2)s^2C_{\phi2} - 2s^2\beta_2kC_{\psi2}\right] \tag{3.24}$$

$$\Sigma_{xy}\Big|_{y=0} = \mu_1\left[(b_1^2-2k^2)s^2C_{\psi1} - 2s^2\alpha_1kC_{\phi1}\right] \\ = \mu_2\left[(b_2^2-2k^2)s^2C_{\psi2} + 2s^2\alpha_2kC_{\phi2}\right] \tag{3.25}$$

Imposing these continuity conditions, we reach the following relation between $P_+(k)$ and $U_-(k)$:

$$J(k)S_+(k) = s^3e^{-s(t_0+kx_0)} + U_-(k) \tag{3.26}$$

where

$$J(k) = -\left[\frac{b_1^2\beta_1(k)}{\mu_1R_1(k)} + \frac{b_2^2\beta_2(k)}{\mu_2R_2(k)}\right] \tag{3.27}$$

where the function $R_n(K)$ is the secular Rayleigh equation:

$$R_n(k) = (b_n^2-2k^2)^2 + 4k^2\alpha_n(k)\beta_n(k) \tag{3.28}$$

of the 'n' material halfspace. The two real roots of this function are the positive and negative inverses of the Rayleigh wave speed of the relevant material, $k = \pm c_n$, where $c_n = 1/c_{R_n}$ with c_{R_n} the relevant Rayleigh wave speed (Eringen and Suhubi, 1975).

Although Wiener–Hopf mandates that $J(k)$ be factorised into two sectionally analytic functions over the negative and positive half spaces, we shall argue that in this case it is not necessary to do so. This is because of the specific form of the displacement jump condition in Eq. (3.15). In effect, this condition is supported over the whole interface except at the point of application, as it prescribes a displacement jump that is 0 everywhere except at $x = x_0, t = t_0$. This is not a half-space condition, but a full space condition. Let us imagine however that we were to achieve the desired product factorisation of $J(k)$:

$$J(k) = J_+(k)J_-(k) \tag{3.29}$$

where $J_+(k)$ is holomorphic for $k>0$ and $J_-(k)$ for $k<0$. Arguably the form of these functions would be similar to that provided in the previous sections for $K(k)$ and $G(k)$ — and indeed, it can be obtained through almost analogous means. Achieving this would allow us to write Eq. (3.26) as

$$J_+(k)P_+(k) = \frac{1}{J_-(k)}\left[s^3e^{-s(t_0+kx_0)} + U_-(k)\right] \tag{3.30}$$

where all that remains is to examine where the term with the exponential is holomorphic. We note that the usual Wiener–Hopf strategy of invoking analytic continuation via Liouville's theorem (Markushevich, 2005a) fails without further consideration, because the function $e^{-s(t_0+kx_0)}$ is not bounded for all $|k| \to \infty$.

Following the method found in Georgiadis and Charalambakis (1994), if we perform the explicit integration of Eq. (3.30). In this case, this approach leads to:

$$\frac{1}{2\pi i}\int_{d-i\infty}^{d+i\infty} J_+(z)S_+(z)\frac{\mathrm{d}z}{z-k} = \\ \frac{1}{2\pi i}\int_{d-i\infty}^{d+i\infty} \frac{s^3e^{-s(t_0+zx_0)}}{J_-(z)}\frac{\mathrm{d}z}{z-k} + \\ + \frac{1}{2\pi i}\int_{d-i\infty}^{d+i\infty} \frac{U_-(z)}{J_-(k)}\frac{\mathrm{d}z}{z-k} \tag{3.31}$$

where d is an arbitrary positive real number. We can then invoke Cauchy's integral formula (Markushevich, 2005b) over each term in the equation, forming closed contours using semi-circles encompassing the positive $\mathrm{Re}[k]>0$ or negative $\mathrm{Re}[k]<0$ half plane.

If we choose a contour closing on the positive half plane for the first term, we find that

$$\frac{1}{2\pi i}\oint_C J_+(z)S_+(z)\frac{\mathrm{d}z}{z-k} = \\ = \int_{d-i\infty}^{d+i\infty} + \int_J \left[J_+(z)S_+(z)\frac{\mathrm{d}z}{z-k}\right] = J_+(k)S_+(k) \tag{3.32}$$

The Jordan integral vanishes. Indeed,

$$\int_J \left[J_+(z) S_+(z) \frac{\mathrm{d}z}{z-k} \right] \to 0 \qquad |z| \to \infty \tag{3.33}$$

where J denotes the Jordan contour over the $\mathrm{Re}[z] > 0$ halfplane. We note that as $|z| \to \infty$ because $J_+(z) \sim z^{1/2}$. In Gurrutxaga-Lerma (2021), we showed that for slipping interfaces in the steady $p_+(x,t) \sim x^{-1/2}$ and some other factors. Thus, by invoking the Tauberian theorem we conclude that $S_+(z) \sim z^{-1}$, and therefore that the integrand vanishes for $\mathrm{Re}[z] > 0$ as $|k| \to \infty$. Thus we reach the expression

$$S_+(k) = \frac{s^3 e^{-s(t_0 + k x_0)}}{J(k)} \tag{3.34}$$

without recourse to the product factorisation of $J(k)$.

3.2.1. Inversion of the fundamental solution to the interfacial traction

The inversion of the interfacial traction $S_+(k)$ can then be achieved via the Cagniard-de Hoop technique (Cagniard, 1939; De Hoop, 1960). We note that the exponential term denotes shifts in time and space; by virtue of properties of the Laplace transform, the s^3 term entails higher order derivatives of the kernel (assuming the motion starts from rest); and the kernel itself, $1/J(k)$ has an analytic form. The spatial inversion is given by the Bromwich integral:

$$\begin{aligned}
\hat{s}_+(x,s) &= \frac{1}{2\pi i} \frac{1}{s^2} \int_{-i\infty}^{i\infty} S_+(k) e^{skx} s \mathrm{d}k \\
&= \frac{1}{2\pi i} \int_{-i\infty}^{i\infty} \frac{1}{J(k)} s^2 e^{-s(t_0 + k x_0)} e^{skx} \mathrm{d}k \\
&= -\frac{s^2 e^{-st_0}}{2\pi i} \int_{-i\infty}^{i\infty} \frac{\mu_1 \mu_2 R_1(k) R_2(k)}{\mu_1 R_1(k) b_2^2 \beta_2(k) + \mu_2 R_2(k) b_1^2 \beta_1(k)} e^{sk(x-x_0)} \mathrm{d}k
\end{aligned} \tag{3.35}$$

The Cagniard-de Hoop procedure requires distorting the integration path via a closed contour of integration. We note that the integrand has branch cuts for $|\mathrm{Re}[k]| > a_1, a_2, b_1, b_2$. The poles due to the denominator are all within the branch cut. Thus, we may conceive of a closed contour of integration formed by: (a) the imaginary axis, (b) a quarter circle on the $\mathrm{Re}[k] > 0, \mathrm{Im}[k] > 0$, (c) a line circuit surrounding the branch cut, and (d) a quarter circle on the $\mathrm{Re}[k] > 0, \mathrm{Im}[k] < 0$. The contribution of the quarter circles vanishes at infinity, because $1/K(k)$ does as $|k| \to \infty$. The contribution of the circuit along the branch cut must therefore equate that along the imaginary axis — the inversion integral itself. Invoking the Schwarz reflection principle (i.e., using $J(\bar{k}) = \bar{J}(k)$), we can write:

$$\hat{s}_+(x,s) = \frac{s^2 e^{-st_0}}{\pi} \int_{a_1}^{\infty} \mathrm{Im}\left[\frac{1}{J(k)} \right] e^{sk(x-x_0)} \mathrm{d}k \tag{3.36}$$

If we change variable to $\tau = -(x - x_0)k$, $\tau \geq 0$, we can rewrite this as:

$$\hat{s}_+(x,s) = -\frac{s^2 e^{-st_0}}{\pi(x-x_0)} \int_{a_1 x}^{\infty} \mathrm{Im}\left[\frac{1}{J\left(-\frac{\tau}{x-x_0}\right)} \right] e^{-s\tau} \mathrm{d}\tau \tag{3.37}$$

This has the form of a forward Laplace transform in τ. Upon applying the Bromwich integral to $\hat{p}_+(x,s)$ in Eq. (3.37), we obtain by inspection (and upon application of the properties of the Laplace transform) the real space solution we seek:

$$\begin{aligned}
&s_+(x - x_0, t - t_0) = \\
&= -\frac{1}{\pi(x-x_0)} \frac{\partial^2}{\partial t^2} \left(\mathrm{Im}\left[\frac{1}{J\left(-\frac{t-t_0}{x-x_0}\right)} \right] \right) \mathrm{H}(t - t_0 - a_1|x|)
\end{aligned} \tag{3.38}$$

The full expression of $\frac{\partial^2}{\partial t^2} \mathrm{Im}\left[\frac{1}{J\left(-\frac{t-t_0}{x-x_0}\right)} \right]$ is given in Appendix B.

3.2.2. Interfacial shear stress due to a general distribution of slip

The interfacial slip $s_+(x,t)$ due to an instantaneous point displacement $u_y(x,t) = \delta(x - x_0, t - t_0)$ can be treated as a fundamental solution with which to obtain the interfacial shear stress due to an arbitrary distribution of slip $u_x(x,t) = \phi(x,t)$ applied over the positive real line. We note here that for finite $t > 0$, the elastodynamic perturbations propagate with either the longitudinal c_l or the tangential c_t speeds of sound, so the support of both $s_+(x,t)$ and $u_-(x,t)$ will be finite and given by $[0, c_l \cdot t]$ for longitudinal and $[0, c_t \cdot t]$ for transverse perturbations. Thus, $\phi(x,t)$ has finite support over a certain interval of $x > 0, t > 0$ and therefore it vanishes for $x < 0$ and is sufficiently differentiable for $x > 0$, which enables us to write

$$\begin{aligned}
s(x,t) &= \int_0^{\infty} \int_0^{\infty} s_+(x - x', t - t') \phi(x', t') \mathrm{d}x' \mathrm{d}t' \\
&\equiv \langle s_+, \phi \rangle
\end{aligned} \tag{3.39}$$

will be the interfacial shear stress due to the distribution of slip $\phi(x,t)$, and $\langle \cdot, \cdot \rangle$ is used to denote the temporal–spatial convolution.

For mathematical convenience, we will rewrite Eq. (3.39) as follows. By construction, the support of $\phi(x,t)$ extends over the positive real line alone in both time and space. We may therefore express $\phi(x,t)$ as (Aki and Richards, 2002):

$$\begin{aligned}
\phi(x,t) = &\int_0^{\infty} \int_0^{\infty} \frac{\partial^2 \phi}{\partial x' \partial t'} \mathrm{H}(x - x') \mathrm{H}(t - t') \mathrm{d}x' \mathrm{d}t' + \\
&+ \phi(0,0)
\end{aligned} \tag{3.40}$$

Now, we assume that $\phi(x, t = 0) = 0$, i.e., that at $t = 0$ the surface has not begun to slip.[1] Thus, $\phi(x,t) = \langle \phi''_{xt}, H(t)H(x) \rangle$ with $\phi''_{xt} \equiv \frac{\partial^2 \phi}{\partial x' \partial t'}$, whereupon

$$\begin{aligned}
s(x,t) &= \langle s_+, \phi \rangle = \langle s_+, \langle \phi''_{xt}, H(t)H(x) \rangle \rangle \\
&= \langle \phi''_{xt}, \langle s_+, H(t)H(x) \rangle \rangle
\end{aligned} \tag{3.41}$$

The term $\langle s_+, H(t)H(x) \rangle$ represents the interfacial shear traction due to a unitary edge dislocation injected at $t = 0$ at the bimaterial interface, and ϕ''_{xt} the distribution of Burgers vector velocities. The dislocation's shear traction is in fact the primitive function:

$$S_+(x,t) = \int_0^{\infty} \int_0^{\infty} s_+(x', t') \mathrm{H}(x - x') \mathrm{H}(t - t') \mathrm{d}x' \mathrm{d}t', \tag{3.42}$$

Using $S_+(x,t)$ is analytically convenient owing to the fact that the kernel depends explicitly on $k \mapsto -t/x$, which enables us to rewrite

$$\frac{1}{x} \frac{\partial^2}{\partial t^2} \left[\mathrm{Im}\left[\frac{1}{J\left(-\frac{t}{x}\right)} \right] \right] = \frac{1}{x} \frac{\partial^2}{\partial t^2} F(k) = \frac{1}{x^3} F''(k) \tag{3.43}$$

Integrating once it t and once in x, one can re-write the primitive function $S_+(x,t)$ as:

$$S_+(k,t) = -\frac{1}{t} F(k) = -\frac{1}{t} F\left(-\frac{t}{x}\right) \tag{3.44}$$

This entails that the convolution in Eq. (3.39) may be rewritten in terms of k:

$$s(k;t) = -\int_0^{\infty} \frac{1}{k - k'} \left[\mathrm{Im}\left[\frac{1}{J(-(k - k'))} \right] \right] v(k';x) \mathrm{d}k' \tag{3.45}$$

where $v(k;x)$ is the interfacial slip velocity, as

$$v(k;x) = \int_0^{\infty} \phi''_{xt}(k;x') \mathrm{d}x' \tag{3.46}$$

4. The bimaterial contact problem

4.1. The uncoupled problem

The slip distribution is necessary to help accommodate the stress mismatch between the frictional and the interfacial shear tractions. In

[1] This assumption would need to change if the motion begins not from rest.

the *uncoupled* problem, the shear and normal tractions do not affect one another: it is assumed that the normal traction does not cause horizontal displacements at the interface, nor does the shear traction cause vertical ones. The sole source of coupling is then the contact condition at the interface, namely Amonton's law, but the tractions involved remain independent from one another. As stated above, under slip, the force balance at the interface requires:

$$q(x,t) + s(x,t) = f\,\mathrm{sign}(f)p(x,t) \tag{4.1}$$

where as before

$$\mathrm{sign}(f) = \frac{[\![\dot{u}_x]\!]}{|[\![\dot{u}_x]\!]|} \tag{4.2}$$

If $q(x,t) < f\,\mathrm{sign}(f)p(x,t)$, then $s(x,t) = 0$, and there is stick. Because $q(x,t)$ involves shear perturbations alone (see Gurrutxaga-Lerma, 2021; Gurrutxaga-Lerma, 2020), the fastest speed at which the shear traction travels is the fastest shear wave speed. The normal traction propagates as fast as the fastest longitudinal speed of sound (by hypothesis, $1/a_1$), which means that $q(x,t) = 0$ for all interfacial points $x > t/a_1$. We call the *head wave region* to the spatial region affected solely by longitudinal waves prior to the arrival of the first transverse wave, i.e., the strip $x \in [t/a_1, t/b_1]$. Naturally, in the uncoupled problem the head wave is trivially in full stick, because the shear traction does not act until the first shear wave arrives at each interfacial point. However, what happens behind this region of stick?

4.2. Can the bimaterial interface sustain uncoupled slip?

Whereas Amonton's law permits the presence of a relative horizontal displacement at the interface (the '*slip*' $u_x(x,t) \equiv \phi(x,t)$), it explicitly requires for contact to be maintained across the interface. In mathematical terms, this entails that Barber (2018)

$$\frac{\partial [\![u_y]\!]}{\partial x} = \frac{\partial u_y^{(1)}}{\partial x} - \frac{\partial u_y^{(2)}}{\partial x} = 0 \tag{4.3}$$

which signifies the contact interface remains vertically compatible during the deformation.

The uncoupled problem cannot satisfy this condition. This is for two reasons. First, there is no general distribution of slip at the uncoupled interface that does not violate condition (4.3). This can be verified from Section 3.2. Consider Eq. (4.3) in terms of the Kelvin potentials:

$$\frac{\partial u_y^{(1)}}{\partial x} - \frac{\partial u_y^{(2)}}{\partial x} = \frac{\partial^2 \phi_1}{\partial x \partial y} - \frac{\partial^2 \phi_2}{\partial x \partial y} - \frac{\partial^2 \psi_1}{\partial x^2} + \frac{\partial^2 \psi_2}{\partial x^2} \tag{4.4}$$

Following Section 3.2, we can express this vertical displacement gradient in Laplace space as:

$$[\![skU_y]\!] = S_+(k)\frac{k^2}{s^2}\left[\frac{\eta_2(k)}{\mu_2 R_2(k)} - \frac{\eta_1(k)}{\mu_1 R_1(k)}\right] \equiv skV(k) \tag{4.5}$$

where $\eta_n(k) = b_n^2 - 2k^2 - 2\alpha_n(k)\beta_n(k)$, $S_+(k)$ the interfacial shear traction (found in Eq. (4.5) convolved with $U_x(k)$) and $[\![skU_y]\!]$ denotes $\frac{\partial u_y^{(1)}}{\partial x} - \frac{\partial u_y^{(2)}}{\partial x}$ in Laplace space.

Clearly, $[\![skU_y]\!] \neq 0$ in general. The only circumstance under which $[\![skU_y]\!] = 0$ is if the two materials across the interface are the same, a case that was studied by this author in Gurrutxaga-Lerma (2020). Otherwise, the bimaterial interface cannot sustain a distribution of slip and remain compatible.

Indeed, a second accessory reason follows from the above: if $[\![skU_y]\!] \neq 0$ for a bimaterial case, it is also true that $[\![U_y]\!] \neq 0$ in general. This provides an indication of how the incompatibility would evolve: the interface will detach if $[\![u_y]\!] > 0$, or interpenetrate if $[\![u_y]\!] < 0$; this will depend on the relative value of the elastic constants, the friction coefficient, and the remote loading conditions. If the interface detaches, Eq. (5.2) becomes invalid as contact is locally lost. Over time, the remote normal load ought to lead to reattachment, at which point a new slip wave would be radiated from the newly established contact region; the loading remaining the same, it appears inevitable that contact would be lost again owing to the same considerations that led to detachment to begin with. If, in turn, the two surfaces meeting at the interface tried to interpenetrate one another (which cannot be), then the interface itself would experience a vertical displacement and wrinkle, leading to oscillatory behaviour. Thus, the uncoupled contact problem is inherently unstable.

That notwithstanding, the validity of the uncoupled assumption as an approximation merits further examination. Indeed, it could remain an acceptable approximation so long as the vertical displacement were small enough to be neglected. However, this is not the case. As can be readily seen in Eq. (4.5) $[\![U_y]\!] \propto V(k)$, which is to say, the vertical displacement is of the same order of magnitude as the interfacial distribution of slip. To wit, the uncoupled problem entails vertical displacements about as large as the horizontal ones. In light of this, the true interfacial tractions will not be accurately captured by the uncoupled problem and, accordingly, neither will the slip distribution itself be adequately modelled: the uncoupled problem is inconsistent.

5. Restoring compatibility via interfacial coupling

Uncoupled slip has been shown to lead to incompatible deformation involving detachment and/or interpenetration along the bimaterial interface. Such instabilities appear to be inherent to bimaterial interfaces, and are evocative of the ones described by Adams (1995, 1998) in sliding contacts under dry friction. In the problem studied by Adams, a wave of slip must exist to accommodate the mismatch between the normal and shear tractions. Similarly, under contact conditions we are discussing here, we ought to expect a slip wavefront propagating away from the edge of the contact zone, as the support of $\phi(x,t)$ (the slip distribution) is bound to increase as the normal and tangential wavefronts expand (cf. Gurrutxaga-Lerma, 2019; Gurrutxaga-Lerma, 2020 for the single material case). The question we wish to answer here is: how can compatibility along a bimaterial interface be restored?

We begin by considering the uncoupled normal and shear tractions acting at the interface as a result of remote normal and shear loads, $p(x,t)$ and $q(x,t)$. These two tractions are the ones given in Section 3.1. The shear traction can only be transferred across the interface according to Amonton's law, so that the mismatch between $p(x,t)$ and $q(x,t)$ need to be correct via a slip distribution $\phi(x,t)$ and the associated tangential shear traction $s(x,t)$ it entails; this was solved in Section 3.2. In a single material medium, these loads are sufficient to solve Eq. (4.3). However, as was argued in Section 4.1, in a bimaterial medium this scheme leads to the violation of compatibility described above. The cause of this violation is that the mismatch in the uncoupled tractions leads to a net elastic vertical displacement across the interface, $[\![u_y]\!] \neq 0$, and an accompanying net vertical gradient $[\![u_{y,x}]\!] = v'_x(x,t) \neq 0$, just as large as the magnitude of the horizontal slip.

To restore compatibility we need to ensure that $[\![u_{y,x}]\!] = 0$. We therefore consider now the following accessory problem: a vertical displacement gradient is applied over the interface, such that the displacement gradient matches the negative of the non-zero incompatible displacement gradient $[\![u_{y,x}]\!] = -v'_x(x,t)$ that caused the incompatibility in the uncoupled problem. We further require that $[\![u_x]\!] = 0$, so as to ensure that all slip is corrective. These two conditions bind the displacements at the interface in such a way that it will result in new corrective normal and tangential tractions, which we denote respectively as $p^*(x,t)$ and $q^*(x,t)$. These tractions can be obtained from the following Wiener–Hopf problem:

$$\begin{aligned} \sigma_{yy}^{(n)}(x,0,t) &= p^*(x,t) \quad x \in \mathbb{R} \\ \sigma_{xy}^{(n)}(x,0,t) &= q^*(x,t) \quad x \in \mathbb{R} \\ [\![u_x(x,0,t)]\!] &\equiv u_x^{(1)}(x,0,t) - u_x^{(2)}(x,0,t) = u_-^*(x,t) \\ [\![u_{y,x}(x,0,t)]\!] &\equiv u_{y,x}^{(1)}(x,0,t) - u_{y,x}^{(2)}(x,0,t) = \end{aligned} \tag{5.1}$$

$$= -v'_x(x,t) + \frac{\partial v^*_-}{\partial x} \quad x \in \mathbb{R}$$

where here $-v'_x(x,t)$ is known from the uncoupled problem, and $v^*_-(x,t)$ is the unknown corrective vertical displacement.

The superposition of the uncoupled problem discussed in Section 3.2 with this new problem restores the compatibility of the interface, but alters the equation of interfacial equilibrium to:

$$|q(x,t) + q^*(x,t) + s(x,t)| = f\,\mathrm{sign}(f)\left(p(x,t) + p^*(x,t)\right), \tag{5.2}$$

which now has additional corrective coupled tractions that are also indirectly dependent on the slip distribution $\phi(x,t)$. In the sequel we show how exactly.

5.1. The compatibility correcting coupled tractions

The tractions $p^*(x,t)$ and $q^*(x,t)$ restore compatibility, but require the solution to a coupled Wiener–Hopf problem. Using the Laplace transforms defined in Eq. (3.19), Eq. (5.2) becomes:

$$\mu_n\left[(b_n^2 - 2a_n^2)s^2\Phi_n + 2\frac{\partial^2\Phi_n}{\partial y^2} - 2sk\frac{\partial\Psi_n}{\partial y}\right]_{y=0} = \frac{P^*(k)}{s^2} \tag{5.3}$$

$$\mu_n\left[2sk\frac{\partial\Phi_n}{\partial y} + \frac{\partial^2\Psi_n}{\partial y^2} - s^2k^2\Psi_n\right]_{y=0} = \frac{Q^*(k)}{s^2} \tag{5.4}$$

$$\left[\left(\frac{\partial\Psi_1}{\partial y} + sk\Phi_1\right) - \left(\frac{\partial\Psi_2}{\partial y} + sk\Phi_2\right)\right]_{y=0} = \frac{U^*_-(k)}{s^3} \tag{5.5}$$

$$\left[\left(\frac{\partial\Phi_1}{\partial y} - sk\Psi_1\right) - \left(\frac{\partial\Phi_2}{\partial y} - sk\Psi_2\right)\right]_{y=0} = \frac{V^*_-(k) - V(k)}{s^3} \tag{5.6}$$

where the sole source term here is given by

$$V(k) = k\left[\frac{\eta_1(k)\mu_2 R_2(k) - \eta_2(k)\mu_1 R_1(k)}{\mu_2 R_2(k) b_1^2\beta_1(k) + \mu_1 R_1(k) b_2^2\beta_2(k)}\right] e^{-s(t_0 + kx_0)} \tag{5.7}$$

when the interfacial displacement u_x is given by the point displacement distribution described in 3.2.

Using the solutions in (3.23), these conditions lead to the following linear system of equations:

$$\begin{bmatrix} k_{11} & k_{12} \\ k_{12} & k_{22} \end{bmatrix} \cdot \begin{bmatrix} P^*(k) \\ Q^*(k) \end{bmatrix} = \begin{bmatrix} U^*_-(k) \\ V^*_-(k) \end{bmatrix} - \begin{bmatrix} 0 \\ V(k) \end{bmatrix} \tag{5.8}$$

where we define the scattering kernel $\mathbf{K}(k)$ as

$$\mathbf{K}(k) = \begin{bmatrix} k_{11} & -k_{12} \\ k_{12} & k_{22} \end{bmatrix} \tag{5.9}$$

with components:

$$k_{11} = -\left[\frac{\alpha_1(k)}{R_1(k)}\frac{b_1^2}{\mu_1} + \frac{\alpha_2(k)}{R_2(k)}\frac{b_2^2}{\mu_2}\right] \tag{5.10}$$

$$k_{22} = -\left[\frac{\beta_1(k)}{R_1(k)}\frac{b_1^2}{\mu_1} + \frac{\beta_2(k)}{R_2(k)}\frac{b_2^2}{\mu_2}\right] \tag{5.11}$$

$$k_{12} = -\left[\frac{\eta_1(k)}{\mu_1 R_1(k)} - \frac{\eta_2(k)}{\mu_2 R_2(k)}\right] \tag{5.12}$$

5.1.1. The product decomposition of the scattering kernel

The resulting system of equations is a Riemann–Hilbert problem, the solution of which requires the factorisation of the scattering kernel into two sectionally analytic factors that satisfy the following representation:

$$\mathbf{K}(k) = \mathbf{K}_-(k)\cdot\mathbf{K}_+(k), \tag{5.13}$$

where $\mathbf{K}_\pm(k)$ ought to be regular and holomorphic over the positive (negative) half-plane of $k \in \mathbb{C}$. As was discussed by the author in Gurrutxaga-Lerma (2021), it is not possible to attain such decomposition owing to the fact that the branch cuts in $\alpha_n(k)$ and $\beta_n(k)$ make the scattering kernel non-commutative. Following Gurrutxaga-Lerma (2021), it is possible to approximate $\mathbf{K}(k)$ via infinite regression to $\mathbf{K}_\pm(k) = \lim_{n\to\infty}\mathbf{K}^n_\pm$.

This approximation, developed by Abrahams in a similar context (Abrahams, 1996, 2000, 2002), relies on swapping the irreducible factor $f(k) = \sqrt{\frac{k_{22}}{k_{11}}}$ with its Padé approximant, $f_n(k) = P_n(k)/Q_n(k)$. This has the effect of substituting the branch cuts preventing the factorisation with discrete poles lying along the former branch cuts; these poles can be regularised as usual (cf. Clancey and Gohberg (2013)), leading to an approximate but very accurate product factorisation of the scattering kernel. The higher the order of the Padé approximant employed is, the more poles it will entail, and the more accurate the resulting Abrahams approximation of the scattering kernel will be. Regardless, the Abrahams approximation retains the asymptotic character of the scattering kernel at $k \to 0$ and $k \to \infty$.

The details regarding how to achieve the Abrahams approximation of Eq. (5.9) can be found in Gurrutxaga-Lerma (2021). Here, we quote those results to state that

$$\mathbf{K}(k) \approx \mathbf{K}^-_{12}(k)\mathbf{D}_n(k)^-\mathbf{D}_n(k)^+\mathbf{K}^+_{12}(k) \tag{5.14}$$

where

$$\mathbf{K}^\pm_{12}(k) = \begin{bmatrix} k^\pm_{12} & 0 \\ 0 & k^\pm_{12} \end{bmatrix}, \quad \text{and} \tag{5.15}$$

$$\mathbf{D}^-_n(k) = \mathbf{C}^-_n(k)\boldsymbol{\Lambda}(k), \quad \mathbf{D}^+_n(k) = \boldsymbol{\Lambda}^{-1}(k)\mathbf{C}^+_n(k)$$

The matrices $\mathbf{C}^\pm_m$ and $\boldsymbol{\Lambda}(k)$ are defined in relation to the order $[n/n]$ Padé approximant of the factor

$$f(k) = \sqrt{\frac{k_{22}}{k_{11}}} \approx f_n(k) = \frac{P_n(k)}{Q_n(k)} \tag{5.16}$$

where $P_n(k)$ and $Q_n(k)$ are two order $2n$ polynomials the coefficients of which can be obtained in the usual way, by matching the Taylor series expansion of $f(k)$ with that of $f_n(k)$ up to order $4n$ (see Baker and Graves Morris, 1996, p.56 onwards).

Obtaining $f_n(k)$ allows us to define $\mathbf{C}^\pm_n$ as:

$$\mathbf{C}^\pm_n(k) = \cos[h_\pm(k)]\mathbf{I} + \sin[h_\pm(k)]\mathbf{J}_n(k) \tag{5.17}$$

where $\mathbf{I}$ is the identity and

$$\mathbf{J}_n(k) = \begin{bmatrix} 0 & -\frac{1}{f_n(k)} \\ f_n(k) & 0 \end{bmatrix}, \qquad f(k) \approx f_n(k) = \frac{P_n(k)}{Q_n(k)}, \tag{5.18}$$

with $h_\pm(k)$ such that

$$h_-(k) + h_+(k) = \arctan h(k), \qquad h(k) = \frac{k_{11}}{k_{12}}\sqrt{\frac{k_{22}}{k_{11}}}, \tag{5.19}$$

The matrix $\boldsymbol{\Lambda}(k)$ is introduced to regularise the poles of $f_n(k)$ and $1/f_n(k)$ in $\mathbf{J}_n(k)$. It is given this form

$$\boldsymbol{\Lambda}(k) = \begin{bmatrix} 1 - \sum_{j=1}^n \frac{c_j}{k-p_j} - \sum_{j=1}^n \frac{d_j}{k+p_j} & -\sum_{j=1}^n \frac{c'_j}{k-p_j} - \sum_{j=1}^n \frac{d'_j}{k+p_j} \\ \sum_{j=1}^n \frac{v'_j}{k-q_j} + \sum_{j=1}^n \frac{w'_j}{k+q_j} & 1 + \sum_{j=1}^n \frac{v_j}{k-q_j} + \sum_{j=1}^n \frac{w_j}{k+q_j} \end{bmatrix} \tag{5.20}$$

where $c_j, c'_j, d_j, d'_j, v_j, v'_j, w_j, w'_j$ are unknown coefficients to be determined so as to guarantee that the poles in $\mathbf{C}_n(k)$ are cancelled. A description of how these coefficients are calculated can be found in Gurrutxaga-Lerma (2021), alongside details regarding the factorisations of $h(k)$ and of k_{12} necessary to obtain $\mathbf{K}_n(k)^\pm = \mathbf{K}^\pm_{12}(k)\mathbf{D}_n(k)^\pm$.

Finally, the factor $k^\pm_{12}(k)$ is the product factorisation of the term

$$k_{12} = k\left[\frac{\eta_1(k)}{\mu_1 R_1(k)} - \frac{\eta_2(k)}{\mu_2 R_2(k)}\right] \implies k_{12} = k^+_{12}\cdot k^-_{12} \tag{5.21}$$

where $\eta_n(k) = b_n^2 - 2k^2 - 2\alpha_n(k)\beta_n(k)$. This factorisation was achieved by the author in Gurrutxaga-Lerma (2021), sec.4.1.3. Here we quote the result:

$$k^\pm_{12}(k) = -k_\pm^{1/2}\frac{k \pm a_1}{R^\pm_2(k)\mu_2}F_\pm(k), \tag{5.22}$$

where $R_2^{\pm}(k)$ is the usual product factorisation of the secular form of the Rayleigh waves (see e.g. Achenbach, 1973 section 9.4.2)

$$\ln F_{\pm}(k) = \left\{ \mp\frac{1}{\pi}\left[\int_{a_1}^{a_2} \arctan m_1(z)\frac{\mathrm{d}z}{z\mp k} + \int_{a_2}^{b_1} \arctan m_2(z)\frac{\mathrm{d}z}{z\mp k} + \int_{b_1}^{b_2} \arctan m_3(z)\frac{\mathrm{d}z}{z\mp k}\right]\right\} \tag{5.23}$$

with the $m_n(z)$ kernels reproduced in Gurrutxaga-Lerma (2021).

5.1.2. The Wiener–Hopf decomposition of the coupled problem

With the scattering matrix decomposed, it is possible to find the Wiener–Hopf decomposition of the matricial problem. Indeed,

$$\mathbf{K}_-(k)\mathbf{K}_+(k)\mathbf{P}_+^*(k) = \mathbf{U}_-^*(k) - \mathbf{V}(k) \tag{5.24}$$

where

$$\mathbf{P}_+(k) = \begin{bmatrix} P^*(k) \\ Q^*(k) \end{bmatrix}, \qquad \mathbf{U}_-(k) = \begin{bmatrix} U_-^*(k) \\ V_-^*(k) \end{bmatrix}, \qquad \mathbf{V}(k) = \begin{bmatrix} 0 \\ V(k) \end{bmatrix} \tag{5.25}$$

Thus,

$$\mathbf{K}_+(k)\mathbf{P}_+^*(k) = [\mathbf{K}_-(k)]^{-1}\mathbf{U}_-^*(k) - [\mathbf{K}_-(k)]^{-1}\mathbf{V}(k) \tag{5.26}$$

All that remains is obtaining the additive factorisation of:

$$[\mathbf{K}_-(k)]^{-1}\mathbf{V}(k) = \frac{1}{|\mathbf{K}_-(k)|}\begin{bmatrix} -K_{12}^-(k)V(k) \\ K_{22}^-(k)V(k) \end{bmatrix} = \mathbf{H}_+(k) + \mathbf{H}_-(k) \tag{5.27}$$

where K_{ij}^- are the elements of $\mathbf{K}_-(k)$.

We achieve a matricial Wiener–Hopf equation of the sort:

$$\mathbf{K}_+(k)\mathbf{P}_+^*(k) + \mathbf{H}_+(k) = \mathbf{E}(k) = = [\mathbf{K}_-(k)]^{-1}\mathbf{U}_-^*(k) - \mathbf{H}_-(k) \tag{5.28}$$

Invoking Liouville's generalised theorem and the expected asymptotic behaviour of the displacements and the tractions at $k \to 0$ and $k \to \infty$, we conclude:

$$\mathbf{K}_+(k)\mathbf{P}_+^*(k) = -\mathbf{H}_+(k) \tag{5.29}$$

$$[\mathbf{K}_-(k)]^{-1}\mathbf{U}_-^*(k) = \mathbf{H}_-(k) \tag{5.30}$$

whereupon the corrective tractions we seek are given by:

$$\mathbf{P}_+^*(k) = -[\mathbf{K}_+(k)]^{-1}\mathbf{H}_+(k) \tag{5.31}$$

5.1.3. The factorisation of $[\mathbf{K}_-(k)]^{-1}\mathbf{V}(k)$

We seek the additive factorisation of

$$[\mathbf{K}_-(k)]^{-1}\mathbf{V}(k) = \mathbf{H}_+(k) + \mathbf{H}_-(k) \tag{5.32}$$

We begin by writing $\mathbf{K}_-(k) = k_{12}^-(k)\mathbf{I}\mathbf{C}^-(k)\boldsymbol{\Lambda}(k)$. Noting that $|\mathbf{C}^-(k)| = 1$ by construction, we find that

$$\mathbf{H}_+(k) + \mathbf{H}_-(k) = \frac{V(k)}{(k_{12}^-)^2|\boldsymbol{\Lambda}(k)|}\begin{bmatrix} -k_{12}^-(C_{11}^-\Lambda_{12} + C_{12}^-\Lambda_{22}) \\ -k_{12}^-(C_{21}^-\Lambda_{12} + C_{22}^-\Lambda_{22}) \end{bmatrix} \tag{5.33}$$

If we perform the additive factorisation of the scalar $V(k) = V_+(k) + V_-(k)$ and use the fact that $C_{ij}^-(k) = C_{ij}^+(-k)$, $k_{12}^+(-k) = k_{12}^-(k)$ and Λ_{ij} has no branch cuts, we find that

$$\mathbf{H}_+(k) = \frac{V_+(k)}{k_{12}^+(-k)|\boldsymbol{\Lambda}(k)|}\begin{bmatrix} -\left[C_{11}^+(-k)\Lambda_{12} + C_{12}^+(-k)\Lambda_{22}\right] \\ C_{21}^+(-k)\Lambda_{12} + C_{22}^+(-k)\Lambda_{22} \end{bmatrix} \tag{5.34}$$

$$\mathbf{H}_-(k) = \frac{V_-(k)}{k_{12}^-(k)|\boldsymbol{\Lambda}(k)|}\begin{bmatrix} -\left[C_{11}^-(k)\Lambda_{12} + C_{12}^-(k)\Lambda_{22}\right] \\ C_{21}^-(k)\Lambda_{12} + C_{22}^-(k)\Lambda_{22} \end{bmatrix} \tag{5.35}$$

whereupon the desired corrective tractions become:

$$\mathbf{P}_+^*(k) = \frac{V_+(k)}{k_{12}^+(k)k_{12}^+(-k)|\boldsymbol{\Lambda}(k)|}\begin{bmatrix} p_1(k) \\ p_2(k) \end{bmatrix} \tag{5.36}$$

with

$$\begin{aligned} p_1(k) &= (C_{11}^+(-k)\Lambda_{12} + C_{12}^+(-k)\Lambda_{22})(C_{22}^+(k)\Lambda_{11} - C_{12}^+(k)\Lambda_{21}) + \\ &\quad + (C_{22}^+(k)\Lambda_{12} - C_{12}^+(k)\Lambda_{22})(C_{21}^+(-k)\Lambda_{12} + C_{22}^+(-k)\Lambda_{22}) \\ p_2(k) &= (C_{11}^+(k)\Lambda_{21} - C_{21}^+(k)\Lambda_{11})(C_{11}^+(-k)\Lambda_{12} + C_{12}^+(-k)\Lambda_{22}) + \\ &\quad + (C_{11}^+(k)\Lambda_{22} - C_{12}^+(k)\Lambda_{12})(C_{21}^+(-k)\Lambda_{12} + C_{22}^+(-k)\Lambda_{22}) \end{aligned} \tag{5.37}$$

This provides us with the corrective tractions in Laplace space. The corrective tractions $P^*(k)$ and $Q^*(k)$ are then the first and second components of $\mathbf{P}_+^*(k)$, respectively.

5.1.4. The additive factorisation of $V(k)$

The additive factorisation of the scalar $V(k)$ requires expressing:

$$V(k) \equiv -ke^{-s(t_0+kx_0)}\left[\frac{\mu_1 R_1\eta_2 - \mu_2 R_2\eta_1}{\mu_1 R_1 b_2^2\beta_2 + \mu_2 R_2 b_1^2\beta_1}\right] = V_+(k) + V_-(k) \tag{5.38}$$

The term $e^{-s(t_0+kx_0)}$ stems from the Dirac delta perturbation on u_x. Had this perturbation been given by the distribution of slip $\phi(x,t)$, the exponential term would be substituted by $\Phi(k;s)$, which is the reason why in the following we rename

$$V(k) = -kv(k)\Phi(k;s), \quad v(k) = \left[\frac{\mu_1 R_1\eta_2 - \mu_2 R_2\eta_1}{\mu_1 R_1 b_2^2\beta_2 + \mu_2 R_2 b_1^2\beta_1}\right] \tag{5.39}$$

where $-k\Phi(k;s)$ is an entire function by construction. Thus, we only require the additive factorisation $v(k) = v_+(k) + v_-(k)$. We can write it formally as

$$v_{\pm}(k) = \mp\frac{1}{2\pi i}\int_{d-i\infty}^{d+i\infty}\frac{v(z)}{z-k}\mathrm{d}z \tag{5.40}$$

The function $v(z)$ has branch cuts we define over the interval $\mathrm{Re}[z] \in [a_1, b_2]$. Examination of the denominator $\mu_1 R_1 b_2^2\beta_2 + \mu_2 R_2 b_1^2\beta_1$ suggests $v(z)$ has a real pole at $|z| = s_2$. The equation $\mu_1 R_1 b_2^2\beta_2 + \mu_2 R_2 b_1^2\beta_1 = 0$ is of course the secular equation for the Stoneley waves, and s_2 denotes the Stoneley wave speed (cf. Eringen and Suhubi (1975),p.540). It is easy to realise that s_2 is bounded[2] by $b_2 < |s_2| < c_2$. The range of existence of this pole depends on the value taken by the ratios μ_1/μ_2, λ_1/λ_2, and ρ_1/ρ_2; this is a question originally examined by Scholte (1947), the conclusion being that the Stoneley waves are non-dissipative, but that their presence is heavily dependent on the relative value of the material constants. For completion, we shall operate under the assumption that a Stoneley wave speed exists; this will lead to an easily identifiable additional term.

Invoking the residue theorem, we have

$$\oint_C \frac{v(z)}{z-k}\mathrm{d}z = 2\pi i\left[\mathrm{Res}[z=s_2] + \mathrm{Res}[z=k]\right] = \int_{d-i\infty}^{d+i\infty} + \int_{\Gamma_+} + \int_{\Gamma_-} + \int_J \tag{5.42}$$

The Jordan integral vanishes upon making the change $z \mapsto Re^{i\theta}$ when $R \to \infty$. The residue at the Stoneley pole can be evaluated explicitly as

$$\mathrm{Res}[z=s_2] = \frac{\mu_1 R_1(s_2)\eta_2(s_2) - \mu_2 R_2(s_2)\eta_1(s_2)}{S(s_2)(s_2-k)} \tag{5.43}$$

[2] The Stoneley pole is a real root of

$$\frac{R_1(z)\beta_2(z)}{R_2(z)\beta_1(z)} = -\frac{\mu_2 b1^2}{\mu_1 b_2^2}. \tag{5.41}$$

For $|z| < a_1$ the LHS is always positive, so no real solution exists. For $a_1 < |z| < b_2$, the LHS is complex and the RHS real, so again no real zero exists. For $|z| > b_2$ the LHS is real, so a real zero could exist. The numerator is always positive, but the denominator is negative before $|z| < c_2$, so if a real zero were to exist, it must do so in $|z| \in [b_2, c_2]$.

where

$$S(k)=\frac{b_2^2\beta_2(k)\mu_1}{\alpha_1(k)\beta_1(k)}\left[4k\left(a_1^2\left(2b_1^2-3k^2\right)+\right.\right.$$
$$+k^2\left(4\left(\alpha_1(k)\beta_1(k)+k^2\right)-3b_1^2\right)\Big)-8b_1^2k\alpha_1(k)\beta_1(k)\Big]+$$
$$+\frac{b_1^2\beta_1(k)\mu_2}{\alpha_2(k)\beta_2(k)}\left[4k\left(a_2^2\left(2b_2^2-3k^2\right)+k^2\left(4\left(\alpha_2(k)\beta_2(k)+k^2\right)-\right.\right.\right.$$
$$-\left.\left.\left.3b_2^2\right)\right)-8b_2^2k\alpha_2(k)\beta_2(k)\Big]-\frac{b_1^2k\mu_2R_2(k)}{\beta_1(k)}-\frac{b_2^2k\mu_1R_1(k)}{\beta_2(k)} \tag{5.44}$$

Finally, the contribution of the $\Gamma_\pm$ segments is reduced to the following three Cauchy integrals:

$$\int_{\Gamma_+}+\int_{\Gamma_-}=\int_{a_1}^{a_2}\frac{f_1(z)}{z-k}\mathrm{d}z+\int_{a_1}^{a_2}\frac{f_2(z)}{z-k}\mathrm{d}z+\int_{a_1}^{a_2}\frac{f_3(z)}{z-k}\mathrm{d}z \tag{5.45}$$

where

$$f_1(k)=\frac{n_1(k)}{d_1(k)},\quad f_2(k)=\frac{n_2(k)}{d_2(k)},\quad f_3(k)=\frac{n_3(k)}{d_3(k)} \tag{5.46}$$

where

$$n_1(k)=-4ib_1^2\sqrt{k^2-a_1^2}\mu_2\left[\left(\mu_2b_2^8+\left(2(\mu_1-4\mu_2)k^2\right.\right.\right.$$
$$+\mu_1\beta_1(k)\beta_2(k)\Big)b_2^6-4k^2\left(3(\mu_1-2\mu_2)k^2-\right.$$
$$-2\alpha_2(k)\beta_2(k)\mu_2+\mu_1\left(-\alpha_2(k)\beta_1(k)+\beta_2(k)\beta_1(k)+\right.$$
$$\left.\alpha_2(k)\beta_2(k)\right)\Big)b_2^4+4k^4\left(-4(\mu_1-\mu_2)a_2^2-8\alpha_2(k)\beta_2(k)\mu_2+\right.$$
$$+2k^2(5\mu_1-6\mu_2)+\mu_1\left(-\alpha_2(k)\right)\beta_1(k)+6\mu_1\alpha_2(k)\beta_2(k)+$$
$$\left.+\mu_1\beta_1(k)\beta_2(k)\Big)b_2^2-\right.$$
$$-16k^6\left(2\left(k^2+\alpha_2(k)\beta_2(k)\right)-a_2^2\right)(\mu_1-\mu_2)\Big)b_1^2+ \tag{5.47}$$
$$+k^2\left(-\mu_2b_2^8-2\left((\mu_1-4\mu_2)k^2+\mu_1\beta_1(k)\beta_2(k)\right)b_2^6+\right.$$
$$4k^2\left(3(\mu_1-2\mu_2)k^2-2\alpha_2(k)\beta_2(k)\mu_2+\right.$$
$$\left.+\mu_1\left(-2\alpha_2(k)\beta_1(k)+2\beta_2(k)\beta_1(k)+\alpha_2(k)\beta_2(k)\right)\right)b_2^4+$$
$$+8k^4\left(2(\mu_1-\mu_2)a_2^2-3\alpha_2(k)\beta_2(k)\mu_1-\beta_1(k)\beta_2(k)\mu_1+\right.$$
$$\left.+k^2(6\mu_2-5\mu_1)+\mu_1\alpha_2(k)\beta_1(k)+4\mu_2\alpha_2(k)\beta_2(k)\right)b_2^2+$$
$$\left.+16k^6(\mu_1-\mu_2)\left(2\left(k^2+\alpha_2(k)\beta_2(k)\right)-a_2^2\right)\right)\Big]$$

$$d_1(k)=b_2^4\left(b_2^2-k^2\right)\mu_1^2b_1^8+$$
$$+\left(\mu_2^2b_2^8+\left(2\beta_1(k)\beta_2(k)\mu_1\mu_2-8k^2\left(\mu_1^2+\mu_2^2\right)\right)b_2^6+\right.$$
$$+8\left(\left(\mu_1^2+3\mu_2^2\right)k^4+\mu_2\left(\mu_1\beta_1(k)\left(\alpha_2(k)-\beta_2(k)\right)+\right.\right.$$
$$\left.\left.+\mu_2\alpha_2(k)\beta_2(k)\right)k^2\right)b_2^4-8k^4\mu_2\left(\mu_1\beta_1(k)\left(\alpha_2-\beta_2\right)+\right.$$
$$+2\mu_2\left(-a_2^2+3k^2+2\alpha_2(k)\beta_2(k)\right)\Big)b_2^2+$$
$$+16k^6\mu_2^2\left(2\left(k^2+\alpha_2(k)\beta_2(k)\right)-a_2^2\right)\Big)b_1^6-$$
$$-k^2\left(\mu_2^2b_2^8-8\left(k^2\left(3\mu_1^2+\mu_2^2\right)-\beta_1(k)\beta_2(k)\mu_1\mu_2\right)b_2^6+\right.$$
$$+8\left(3\left(\mu_1^2+\mu_2^2\right)k^4+\mu_2\left(4\mu_1\beta_1(k)\left(\alpha_2(k)-\beta_2(k)\right)+\right.\right.$$
$$\left.\left.+\mu_2\alpha_2(k)\beta_2(k)\right)k^2\right)b_2^4- \tag{5.48}$$
$$-16k^4\mu_2\left(2\mu_1\beta_1(k)\left(\alpha_2(k)-\beta_2(k)\right)+\right.$$
$$\left.+\mu_2\left(-a_2^2+3k^2+2\alpha_2(k)\beta_2(k)\right)\right)b_2^2+$$
$$+16k^6\mu_2^2\left(2\left(k^2+\alpha_2(k)\beta_2(k)\right)-a_2^2\right)\Big)b_1^4-$$
$$-8b_2^2k^4\mu_1\left(\left(2k^2\mu_1-\beta_1(k)\beta_2(k)\mu_2\right)b_2^4+\right.$$
$$+2a_1^2\left(b_2^2-k^2\right)\mu_1b_2^2-$$
$$-2k^2\left(\mu_1k^2+2\mu_2\beta_1(k)\left(\alpha_2(k)-\beta_2(k)\right)\right)b_2^2+$$
$$+4k^4\mu_2\beta_1(k)\left(\alpha_2(k)-\beta_2(k)\right)\Big)b_1^2+$$
$$\left.+\ 16a_1^2b_2^4k^6\left(b_2^2-k^2\right)\mu_1^2\right.$$

$$n_2(k)=4ib_1^2\sqrt{k^2-a_1^2}\mu_2\left[\left(\mu_2b_2^8+\left(2(\mu_1-4\mu_2)k^2\right.\right.\right.$$
$$+\mu_1\beta_1(k)\beta_2(k)\Big)b_2^6-4k^2\left(3(\mu_1-2\mu_2)k^2-\right.$$
$$-2\bar\alpha_2(k)\beta_2(k)\mu_2+\mu_1\left(-\bar\alpha_2(k)\beta_1(k)+\beta_2(k)\beta_1(k)+\right.$$
$$\left.\bar\alpha_2(k)\beta_2(k)\right)\Big)b_2^4+4k^4\left(-4(\mu_1-\mu_2)a_2^2-8\bar\alpha_2(k)\beta_2(k)\mu_2+\right.$$
$$+2k^2(5\mu_1-6\mu_2)+\mu_1\left(-\bar\alpha_2(k)\right)\beta_1(k)+6\mu_1\bar\alpha_2(k)\beta_2(k)+$$
$$\left.+\mu_1\beta_1(k)\beta_2(k)\Big)b_2^2-\right.$$
$$-16k^6\left(2\left(k^2+\bar\alpha_2(k)\beta_2(k)\right)-a_2^2\right)(\mu_1-\mu_2)\Big)b_1^2+ \tag{5.49}$$
$$+k^2\left(-\mu_2b_2^8-2\left((\mu_1-4\mu_2)k^2+\mu_1\beta_1(k)\beta_2(k)\right)b_2^6+\right.$$
$$4k^2\left(3(\mu_1-2\mu_2)k^2-2\bar\alpha_2(k)\beta_2(k)\mu_2+\right.$$
$$\left.+\mu_1\left(-2\bar\alpha_2(k)\beta_1(k)+2\beta_2(k)\beta_1(k)+\bar\alpha_2(k)\beta_2(k)\right)\right)b_2^4+$$
$$+8k^4\left(2(\mu_1-\mu_2)a_2^2-3\bar\alpha_2(k)\beta_2(k)\mu_1-\beta_1(k)\beta_2(k)\mu_1+\right.$$
$$\left.+k^2(6\mu_2-5\mu_1)+\mu_1\bar\alpha_2(k)\beta_1(k)+4\mu_2\bar\alpha_2(k)\beta_2(k)\right)b_2^2+$$
$$\left.+16k^6(\mu_1-\mu_2)\left(2\left(k^2+\bar\alpha_2(k)\beta_2(k)\right)-a_2^2\right)\right)\Big]$$

$$d_2(k)=b_2^4\left(b_2^2-k^2\right)\mu_1^2b_1^8+$$
$$+\left(\mu_2^2b_2^8+\left(2\beta_1(k)\beta_2(k)\mu_1\mu_2-8k^2\left(\mu_1^2+\mu_2^2\right)\right)b_2^6+\right.$$
$$+8\left(\left(\mu_1^2+3\mu_2^2\right)k^4+\mu_2\left(\mu_1\beta_1(k)\left(\bar\alpha_2(k)-\beta_2(k)\right)+\right.\right.$$
$$\left.\left.+\mu_2\bar\alpha_2(k)\beta_2(k)\right)k^2\right)b_2^4-8k^4\mu_2\left(\mu_1\beta_1(k)\left(\alpha_2-\beta_2\right)+\right.$$
$$+2\mu_2\left(-a_2^2+3k^2+2\bar\alpha_2(k)\beta_2(k)\right)\Big)b_2^2+$$
$$+16k^6\mu_2^2\left(2\left(k^2+\bar\alpha_2(k)\beta_2(k)\right)-a_2^2\right)\Big)b_1^6-$$
$$-k^2\left(\mu_2^2b_2^8-8\left(k^2\left(3\mu_1^2+\mu_2^2\right)-\beta_1(k)\beta_2(k)\mu_1\mu_2\right)b_2^6+\right.$$
$$+8\left(3\left(\mu_1^2+\mu_2^2\right)k^4+\mu_2\left(4\mu_1\beta_1(k)\left(\bar\alpha_2(k)-\beta_2(k)\right)+\right.\right.$$
$$\left.\left.+\mu_2\bar\alpha_2(k)\beta_2(k)\right)k^2\right)b_2^4- \tag{5.50}$$
$$-16k^4\mu_2\left(2\mu_1\beta_1(k)\left(\bar\alpha_2(k)-\beta_2(k)\right)+\right.$$
$$\left.+\mu_2\left(-a_2^2+3k^2+2\bar\alpha_2(k)\beta_2(k)\right)\right)b_2^2+$$
$$+16k^6\mu_2^2\left(2\left(k^2+\bar\alpha_2(k)\beta_2(k)\right)-a_2^2\right)\Big)b_1^4-$$
$$-8b_2^2k^4\mu_1\left(\left(2k^2\mu_1-\beta_1(k)\beta_2(k)\mu_2\right)b_2^4+\right.$$
$$+2a_1^2\left(b_2^2-k^2\right)\mu_1b_2^2-$$
$$-2k^2\left(\mu_1k^2+2\mu_2\beta_1(k)\left(\bar\alpha_2(k)-\beta_2(k)\right)\right)b_2^2+$$
$$+4k^4\mu_2\beta_1(k)\left(\bar\alpha_2(k)-\beta_2(k)\right)\Big)b_1^2+$$
$$+\ 16a_1^2b_2^4k^6\left(b_2^2-k^2\right)\mu_1^2$$

$$n_3(k)=2ib_1^2\sqrt{k^2-a_1^2}\mu_2\left[\left(\mu_2b_2^8+\left(2(\mu_1-4\mu_2)k^2\right.\right.\right.$$
$$+\mu_1\bar\beta_1(k)\beta_2(k)\Big)b_2^6-4k^2\left(3(\mu_1-2\mu_2)k^2-\right.$$
$$-2\bar\alpha_2(k)\beta_2(k)\mu_2+\mu_1\left(-\bar\alpha_2(k)\bar\beta_1(k)+\beta_2(k)\bar\beta_1(k)+\right.$$
$$\left.\bar\alpha_2(k)\beta_2(k)\right)\Big)b_2^4+4k^4\left(-4(\mu_1-\mu_2)a_2^2-8\bar\alpha_2(k)\beta_2(k)\mu_2+\right.$$
$$+2k^2(5\mu_1-6\mu_2)+\mu_1\left(-\bar\alpha_2(k)\right)\bar\beta_1(k)+6\mu_1\bar\alpha_2(k)\beta_2(k)+$$
$$\left.+\mu_1\bar\beta_1(k)\beta_2(k)\Big)b_2^2-\right.$$
$$-16k^6\left(2\left(k^2+\bar\alpha_2(k)\beta_2(k)\right)-a_2^2\right)(\mu_1-\mu_2)\Big)b_1^2+ \tag{5.51}$$
$$+k^2\left(-\mu_2b_2^8-2\left((\mu_1-4\mu_2)k^2+\mu_1\bar\beta_1(k)\beta_2(k)\right)b_2^6+\right.$$
$$4k^2\left(3(\mu_1-2\mu_2)k^2-2\bar\alpha_2(k)\beta_2(k)\mu_2+\right.$$
$$\left.+\mu_1\left(-2\bar\alpha_2(k)\bar\beta_1(k)+2\beta_2(k)\bar\beta_1(k)+\bar\alpha_2(k)\beta_2(k)\right)\right)b_2^4+$$
$$+8k^4\left(2(\mu_1-\mu_2)a_2^2-3\bar\alpha_2(k)\beta_2(k)\mu_1-\bar\beta_1(k)\beta_2(k)\mu_1+\right.$$
$$\left.+k^2(6\mu_2-5\mu_1)+\mu_1\bar\alpha_2(k)\bar\beta_1(k)+4\mu_2\bar\alpha_2(k)\beta_2(k)\right)b_2^2+$$
$$\left.+16k^6(\mu_1-\mu_2)\left(2\left(k^2+\bar\alpha_2(k)\beta_2(k)\right)-a_2^2\right)\right)\Big]$$

$$
\begin{aligned}
d_3(k) = {} & b_2^4\left(b_2^2-k^2\right)\mu_1^2 b_1^8 + \\
& + \left(\mu_2^2 b_2^8 + \left(2\bar{\beta}_1(k)\beta_2(k)\mu_1\mu_2 - 8k^2\left(\mu_1^2+\mu_2^2\right)\right) b_2^6 + \\
& + 8\left(\left(\mu_1^2+3\mu_2^2\right)k^4 + \mu_2\left(\mu_1\bar{\beta}_1(k)\left(\bar{\alpha}_2(k)-\beta_2(k)\right) + \right.\right. \\
& \left.\left. + \mu_2\bar{\alpha}_2(k)\beta_2(k)\right)k^2\right) b_2^4 - 8k^4\mu_2\left(\mu_1\bar{\beta}_1(k)\left(\alpha_2-\beta_2\right) + \right. \\
& \left. + 2\mu_2\left(-a_2^2+3k^2+2\bar{\alpha}_2(k)\beta_2(k)\right)\right) b_2^2 + \\
& + 16k^6\mu_2^2\left(2\left(k^2+\bar{\alpha}_2(k)\beta_2(k)\right)-a_2^2\right)\right) b_1^6 - \\
& - k^2\left(\mu_2^2 b_2^8 - 8\left(k^2\left(3\mu_1^2+\mu_2^2\right) - \bar{\beta}_1(k)\beta_2(k)\mu_1\mu_2\right) b_2^6 + \right. \\
& + 8\left(3\left(\mu_1^2+\mu_2^2\right)k^4 + \mu_2\left(4\mu_1\bar{\beta}_1(k)\left(\bar{\alpha}_2(k)-\beta_2(k)\right) + \right.\right. \\
& \left.\left. + \mu_2\bar{\alpha}_2(k)\beta_2(k)\right)k^2\right) b_2^4 - \\
& - 16k^4\mu_2\left(2\mu_1\bar{\beta}_1(k)\left(\bar{\alpha}_2(k)-\beta_2(k)\right) + \right. \\
& \left. + \mu_2\left(-a_2^2+3k^2+2\bar{\alpha}_2(k)\beta_2(k)\right)\right) b_2^2 + \\
& + 16k^6\mu_2^2\left(2\left(k^2+\bar{\alpha}_2(k)\beta_2(k)\right)-a_2^2\right)\right) b_1^4 - \\
& - 8b_2^2k^4\mu_1\left(\left(2k^2\mu_1 - \bar{\beta}_1(k)\beta_2(k)\mu_2\right) b_2^4 + \right. \\
& + 2a_1^2\left(b_2^2-k^2\right)\mu_1 b_2^2 - \\
& - 2k^2\left(\mu_1 k^2 + 2\mu_2\bar{\beta}_1(k)\left(\bar{\alpha}_2(k)-\beta_2(k)\right)\right) b_2^2 + \\
& \left. + 4k^4\mu_2\bar{\beta}_1(k)\left(\bar{\alpha}_2(k)-\beta_2(k)\right)\right) b_1^2 + \\
& + 16a_1^2 b_2^4 k^6\left(b_2^2-k^2\right)\mu_1^2
\end{aligned}
\tag{5.52}
$$

where $\bar{\alpha}_i(k) = \sqrt{k^2-a_i^2}$ and $\bar{\beta}_i(k) = \sqrt{k^2-b_i^2}$.

This leads to the additive factorisation of $v(k)$:

$$
\begin{aligned}
v_{\pm}(k) = {} & \mp\frac{1}{2\pi i}\left[\int_{a_1}^{a_2}\frac{f_1(z)}{z-k}\mathrm{d}z + \int_{a_1}^{a_2}\frac{f_2(z)}{z-k}\mathrm{d}z + \int_{a_1}^{a_2}\frac{f_3(z)}{z-k}\mathrm{d}z\right] - \\
& - \frac{1}{s_2-k}\frac{\mu_1 R_1(s_2)\eta_2(s_2) - \mu_2 R_2(s_2)\eta_1(s_2)}{S(s_2)}
\end{aligned}
\tag{5.53}
$$

By extension, we achieve that of $V(k)$ as $V_{\pm}(k) = -k\Phi(k)v_{\pm}(k)$.

5.2. Inversion of the corrective tractions

The inversion of $P^*(k)$ and $Q^*(k)$ can be achieved using the same Cagniard-de Hoop procedure we outlined in Section 3.2.1. This results in

$$
p^*(x,t) = -\frac{1}{\pi}\frac{1}{x}\frac{\partial^2}{\partial t^2}\left[\mathrm{Im}\left[P^*\left(-\frac{t}{x}\right)\right]\right] \tag{5.54}
$$

$$
q^*(x,t) = -\frac{1}{\pi}\frac{1}{x}\frac{\partial^2}{\partial t^2}\left[\mathrm{Im}\left[Q^*\left(-\frac{t}{x}\right)\right]\right] \tag{5.55}
$$

This inversion completes the obtention of the explicit normal and shear traction corrections that guarantee compatibility at the bimaterial interface.

From the explicit formulae above it is possible to deduce a number of features to be expected from the solution, chiefly related to their wave structure and sign. First, both p^* and q^* comprise both longitudinal and shear wavefronts, the fastest of which travels at the fastest longitudinal speed of the bimaterial system, $1/a_1$, in both cases. This is because both corrective tractions are triggered in response to the fastest waves travelling across the interface, and so is the slip wave and, by extension, the need for compatibility (see Eq. (4.5)). Second, if the bimaterial system supports Stoneley waves, their effect is one of reversing the sign of the traction wave's amplitude behind. This is because asymptotically, the near field of the Stoneley wave front involves terms of the form $1/(t-s_2x)^3$ as entailed by the term $-k/(s_2-k)$ upon inversion. This situation is analogous to that found in Gurrutxaga-Lerma (2021) in relation to the effect Rayleigh waves have in single material interfaces. In both cases, the effect is that of bringing about a narrow region of reverse slip ahead of the Stoneley (or, for single materials, Rayleigh) wave, but behind the head wave. If the interface can support Stoneley waves, then the reverse slip region is narrower, as the Stoneley wave speed is slightly higher than the Rayleigh wave speed.

5.3. The corrected governing equation

The governing equation of the contact problem is an expression of Amonton's law, whereby

$$
|q(x,t) + q^*(x,t) + s(x,t)| = f\,\mathrm{sign}(f)\left(p(x,t) + p^*(x,t)\right) \tag{5.56}
$$

Crucially, both $q^*(x,t)$ and $s(x,t)$ are convolutions of a bimaterial kernel with the distribution of slip, which can be grouped together:

$$
q^*(x,t) + s(x,t) = \langle \phi(x,t), Q(x,t)\rangle \tag{5.57}
$$

where $Q(x,t)$ can be obtained from summing over the convolution kernels $s_+(x,t)$ and $Q^*(x,t)$ given, respectively, in Eqs. (3.38) and (5.55). We note however that the corrective normal traction depends on $\phi(x,t)$ too as $p^*(x,t) = \langle \phi(x,t), P^*(x,t)\rangle$, that is to say, that now both sides of the equation depend on $\phi(x,t)$, the distribution of slip. It is nevertheless possible to solve this equation numerically via collocation. The details of the procedure are given in Appendix C; in the next section we focus on the physical implications of the coupled problem instead.

6. Stability of the compatible problem

We wish to determine whether there are loading or material conditions under which the interface detaches. In principle, the governing equation of the contact problem (Eq. (5.56)) cannot tell us whether interfacial detachment takes place, because the equation itself is invalid under separation. However, Eq. (5.56) itself can be in contradiction with the attachment condition that $p(x,t) + p^*(x,t) > 0$: if the latter is found to be violated by the former, this would be suggestive of interfacial separation in the compatible problem.

Thus, let us assume that the interface is operating under forward slip, so that $q(x,t) + q^*(x,t) + s(x,t) > 0$ and that $p(x,t) + p^*(x,t) > 0$. In that case, Eq. (5.56) can be worked in Laplace space:

$$
\begin{aligned}
& s^2\Phi(k)\left[S_+(k) + Q^*(k) - fP^*(k)\right] = fP(k) - Q(k) \implies \\
& \implies s^2\Phi(k) = \frac{fP(k) - Q(k)}{S_+(k) + Q^*(k) - fP^*(k)}
\end{aligned}
\tag{6.1}
$$

If assuming forward slip[3] the contact pressure changes sign, i.e., $p(x,t) + p^*(x,t) \le 0$. In Laplace space, the left hand side of this condition takes the form $P(k) + s^2\Phi(k)P^*(k)$, and assuming Eq. (5.56) remains valid, we may define the auxiliary function

$$
X(k) = P(k) - P^*(k)\frac{fP(k) - Q(k)}{fP^*(k) - Q^*(k) - S_+(k)} \tag{6.2}
$$

the inverse of which takes the form

$$
\chi(x,t) = -\frac{1}{\pi}\frac{1}{x}\frac{\partial^2}{\partial t^2}\mathrm{Im}\left[X\left(-\frac{t}{x}\right)\right] \tag{6.3}
$$

Examining $\chi(x,t)$, it is possible to determine whether a specific interface will detach owing to a violation of the contact conditions, if $\chi(x,t) < 0$ anywhere in its domain. Given that contact is established only for $t > 0, x > 0$, we may introduce the auxiliary collective variable $k = -t/x$ so that we need only test $-\pi x^3\chi(x,t) := \chi(k) > 0$ as given by

$$
\chi(k) = \frac{\partial^2}{\partial k^2}\mathrm{Im}\left[X(k)\right], \qquad k < 0 \tag{6.4}
$$

Thus, separation occurs if $\chi(k) > 0$ (with $k = -t/x$), that is, separation occurs if $\mathrm{Im}\left[X(k)\right]$ is concave.

6.1. Transient causes of interfacial detachment

Testing whether $\chi(k) > 0$ for $k < 0$ under specific combinations of loading and interfacial constants provides a direct way for establishing whether the bimaterial interface will experience a transient detachment. There are nevertheless a vast number of factors to consider,

[3] The same situation arises under reverse slip.

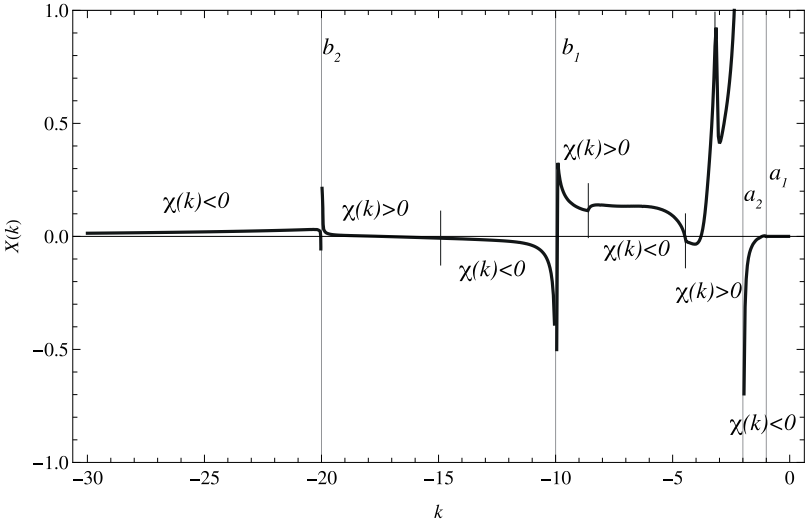

Fig. 2. The Im$[X(k)]$ function when $a_1 = 1$, $a_2 = 2$, $b_1 = 10$, $b_2 = 20$, $\mu_1 = 1$, $\mu_2 = 1$, $\varphi = 1$.

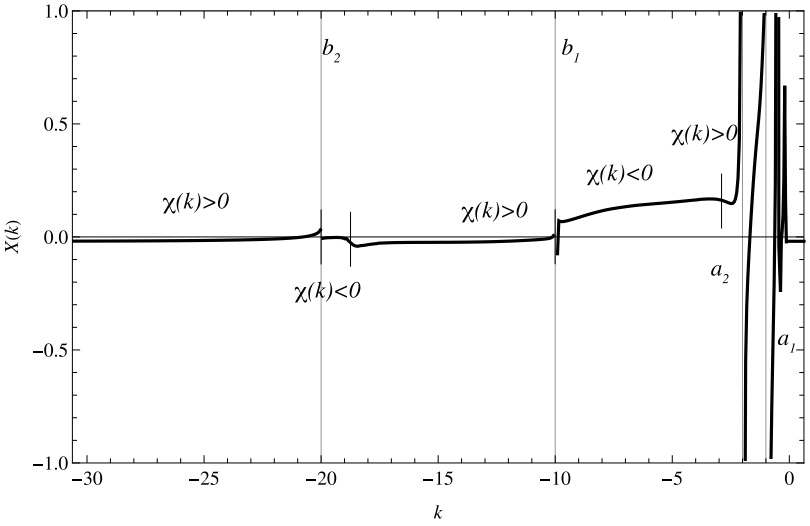

Fig. 3. The Im$[X(k)]$ function when $a_1 = 1$, $a_2 = 2$, $b_1 = 10$, $b_2 = 20$, $\mu_1 = 1$, $\mu_2 = 1$, $\varphi = 0.01$.

including the relative values of the elastic constants in both materials, the frictional coefficient, and the loading intensity. For simplicity, in the following we explore a number of such cases only, and draw some general conclusions based on them. We will also define the frictional factor

$$\varphi = f\frac{P_0}{Q_0} \tag{6.5}$$

to relate friction coefficient to the remote loading's magnitude.

There are two distinct circumstances under which detachment might be expected: (1) in the near field (i.e., for k finite), which would correspond to a transient local detachment; (2) in the far field, as $|k| \to \infty$, which would correspond to a detachment once transient loading has subsided and the steady state has been reached. Local examination of the form of Im$[X(k)]$ in a number of loading and materials conditions showcases that a typical transient loading entails regions of attachment and detachment in quick succession as the interfacial tractional waves propagate at the different speeds of sound. Two cases are examined here in detail: (a) with relatively similar elastic constants, $\mu_1 = 1 = \mu_2$, $\lambda_1 = 98 = \lambda_2$, but $\rho_1 = 100$, $\rho_2 = 400$ (Figs. 2 and 3); and (b) with relatively dissimilar elastic constants $\mu_1 = 1$, $\mu_2 = 10$, $\lambda_1 = 7$, $\lambda_2 = 20$, but $\rho_1 = 9$, $\rho_2 = 160$ (Figs. 4 and 5); and for large and small frictional factors ϕ.

6.1.1. General causes of detachment

We begin by noting that in the current framework detachment is brought about by the action of either the coupling corrective tractions, or the slip distribution. For a compressive remote normal load, $\partial_k^2 \text{Im}[X(k)]$ changes sign only if $\partial_k^2 \text{Im}[\frac{f P(k) - Q(k)}{f P^*(k) - Q^*(k) - S_+(k)}]$ does so. So long as the interface remains unaffected by either the shear traction $Q(k)$, the slip distribution's corrective traction $S_+(k)$ or the coupling shear traction $Q^*(k)$, the interface cannot detach. This means that detachment is intimately related to the structure of the transient solution at the interface. The solution comprises four wave fronts: two longitudinal wavefronts, corresponding to the first and second material's longitudinal speed of sounds ($1/a_1$ and $1/a_2$ respectively); and two shear wavefronts, corresponding to the first and second material's transverse speed of sounds ($1/b_1$ and $1/b_2$ respectively). These wavefronts are launched as the transient remote load reaches the interface, and are sustained by the two material media, meaning that in the transient those parts of the bimaterial medium that propagate elastic waves at the lowest speeds are initially subjected to super- and transonic loads.

Were the normal and shear tractions to be uncoupled, they would propagate independently of one another with the longitudinal and transverse wavefronts respectively (cf. Gurrutxaga-Lerma, 2019), and as was discussed in Section 4.1, the solution would remain in trivial

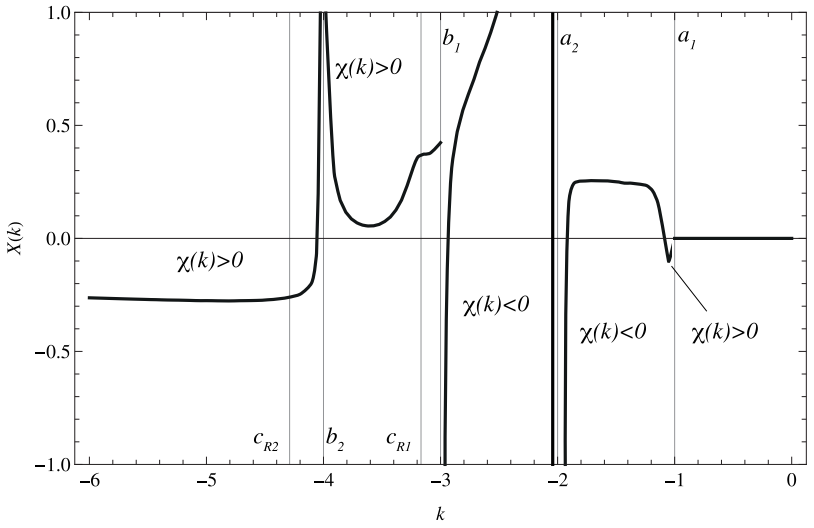

Fig. 4. The Im[$X(k)$] function when $a_1 = 1$, $a_2 = 2$, $b_1 = 3$, $b_2 = 4$, $\mu_1 = 1$, $\mu_2 = 10$, $\varphi = 0.01$.

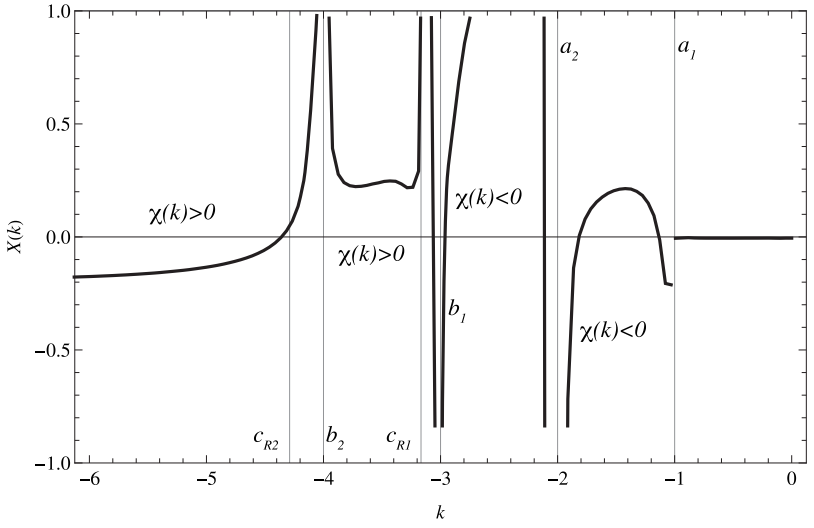

Fig. 5. The Im[$X(k)$] function when $a_1 = 1$, $a_2 = 2$, $b_1 = 3$, $b_2 = 4$, $\mu_1 = 1$, $\mu_2 = 1$, $\varphi = 1$.

stick in the head wave's region, which in the uncoupled problem would run from $|k| \in [a_1, b_1]$. However, owing to the coupling, this is not longer the case: if we examine the form of the coupled shear traction $Q^*(k)$ in Eq. (5.36), it is amply clear that it shares the same inherent mathematical structure as the normal load. In particular, it is affected by the same $|k| > a_1, a_2, b_1, b_2$ branch cuts and the same poles as $P^*(k)$ is; this entails tractional terms launched with both longitudinal and transverse propagation speeds. Therefore, unlike $Q(k)$, the coupled corrective traction $Q^*(k)$ begins its propagation with the first longitudinal wavefront. This is sufficient to cause slip even when the loading is nominally normal alone, as it entails the presence of a non-zero shear term in the force balance (Eq. (5.56)); thus, the interface is no longer trivially stuck in the head wave region existing between the arrival of the first longitudinal wave and the first transverse wavefront, something that contrast sharply with the unimaterial case (or indeed, with any uncoupled problem), where the head wave region is always a region of stick (Gurrutxaga-Lerma, 2019; Gurrutxaga-Lerma, 2020) because it sees no shear tractions acting on it.

6.1.2. Detachment in the near field

As a consequence, both slip and interfacial detachment are possible even before the first shear wavefront arrives at a given interfacial point interface. This is indeed observed in the loading cases studied here. In particular, for the contact problem between elastically similar materials shown in Figs. 2 and 3, detachment is locally predicted for $k < -a_2$; in Figs. 4 and 5, which concern the corresponds to the elastically dissimilar materials, there is also a narrow region of local detachment just after the first longitudinal wavefront arrives, for $k < -a_1$. In all cases, the detachment at the head wave is caused by the elastic mismatch at the interface triggering a supersonic loading in the medium with lower speeds of sound (in the cases shown here, medium 2). This effect is particularly strong when the materials are elastically similar (cases shown in Figs. 2 and 3), because by construction the speeds of sound in this situation are very different and, as a result, medium 2 is required to sustain super and transonic loads for longer.

6.1.3. Detachment in the far field

Once the effects of the transient have subsided and if the materials in contact are relatively similar (cases shown in Figs. 2 and 3), local detachment is predicted in the transient but not necessarily in the far field. In this case, detachment in the far field (meaning for long times, i.e., in the steady state) is expected only if the remote normal load is sufficiently weak that normal corrective tractions at the interface (brought about by the coupling) can violate the contact condition;

indeed, when $\varphi = 0.01$ is very low (Fig. 3), the interface is predicted to detach as $k \to -\infty$, a situation not mirrored when, caeteris paribus, $\varphi = 1$ is sufficiently large (Fig. 3). This behaviour has been observed for other combinations of relatively similar elastic constants (not shown here in the interest of brevity), and is largely explained by the fact expressed above: contact can be lost if the remote pressure load is sufficiently weak that the corrective normal traction brought about by the shear coupling can overcome that due to the remote normal load. This detachment would also occur if, for a given nominally stable loading, the interfacial frictional coefficient became sufficiently low. In this case, this would happen because when the friction coefficient is low, the interface transmits shear loads weakly, which entails wide regions of stick at the interface and these, through the coupling, tend to lead to positive normal tractions in order for both sides of Eq. (5.56) to remain balanced.

6.1.4. Local detachments

Beyond that, the contact interface between similar materials can also experience local, transient detachment. This is also indicated in Figs. 2 and 3; in both cases, transient detachment is predicted in the near field upon the arrival of the longitudinal wavefronts. For low φ frictional factors, the possibility of detachment upon the arrival of the first shear wave is also reported; for high φ frictional factors, detachment is postponed until the arrival of the second longitudinal wavefront. The reasons for this behaviour are grounded, as was explained above, on the coupling: the longitudinal fronts trigger a corrective shear traction and a slip distribution is necessary to ensure Coulomb's law is satisfied locally. This, in turn, means that a corrective normal traction will arise that may flip the sign of the remote load's normal traction, more dramatically for low values of φ.

In principle, once detachment has been predicted for some value of $k = k_0$, the solution becomes invalid for all $|k| > k_0$: as the contact conditions have been violated, Eq. (5.56) becomes invalid thereafter, and the interface becomes a free surface. Thus, what we have so far referred to as 'transient detachment' could seem to be a misnomer: the loss of contact during the transient appears to be inevitable, with nothing beyond the transient nature of the loading suggestive of a transient loss of contact. However, this is necessarily the case: unlike the detachment predictions in the far field of k, transient detachment does not appear to be due to an inherent instability. This is because once detachment occurs, the chief cause for it – the coupling corrective tractions – cease to act, and the remote pressure becomes once again the sole acting normal load. If the normal load had originally sufficed to ensure compatibility at the interface, and it was only because of the action of the corrective tractions that contact was lost, then it stands to reason that once the corrective tractions cease to exist the normal load will in principle ensure contact would be regained.

6.1.5. Resumption of contact

Thus, the remote normal load alone would ensure that eventually the two interfaces regain contact. Once this happens, we are faced with a challenging, highly non-linear problem: parts of the interface will not have yet detached, parts will have, and some will have just regained contact whilst others remain detached. The interfacial tractions at that point will comprise two different contributions: those launched by the rest of the interface, whether in contact or not, and those diffracted by the newly attached interface. Those of the newly attached interface would be mathematically captured by the formulation presented here. Those of the rest of the interface will be highly dependent on its current and past history, and prompt a highly non-linear problem that falls out of the scope of this work. Depending on its nature, it appears likely that once contact is regained, it may again be lost due to the coupling. If that is the case, we would in effect be triggering waves of detachment of the sort investigated by e.g. Schallamach (1971). Still, it seems clear that local transient detachment can be overcome, particularly if a sufficiently strong remote normal load is applied, and the solutions we have derived here offer a succinct way of examining whether and where it will happen.

As stated above, when the materials meeting at the interface are relatively dissimilar (cases discussed in Figs. 4 and 5), local transient detachments are only predicted for small regions behind the arrival of the first longitudinal wavefront. However, in this case the two loading cases examined here predict detachment in the far field irrespective of the magnitude of loading (two orders of magnitude larger for Fig. 5 than Fig. 4). That is, whereas for similar materials detachment at the interface could be remedied with stronger contact forces, for the dissimilar case detachment appears inevitable once the interface begins to be loaded with shear waves irrespective of the external loads' magnitude. The reasons for this instability are, again, rooted in the coupling's effect in the far field: when the elastic constants are sufficiently dissimilar, it is possible for the corrective coupled traction $p^*(x,t)$ to overcome the magnitude of the uncoupled traction $p(x,t)$ and revert its sign. In effect, this happens because the interface is forced to slip considerably to accommodate the mismatch, and in so doing the sign of the normal traction is reversed. The situation is more problematic than transient detachments because no load combination appears able to avoid it, and because once the detachment has taken place, even if the remote normal load leads to re-attachment, this will eventually lead to further detachment as the effects of the transient subsidise and large values of $|k| = t/x$ are achieved: over sufficiently long times, the interface would eventually reach the steady state of detachment predicted here. Such behaviour is reminiscent of the Adams instabilities (Adams, 1995).

6.1.6. Summary

In general, albeit the detachment depends on a combination of factors including the magnitude of the remote loading, the relative values of the elastic constants and the frictional coefficients, there are a number of conditions that promote interfacial detachment:

(1) Disparity in the elastic constants: if the materials at either side of the bimaterial interface have very dissimilar elastic moduli, the interface is more likely to destabilise and display detachment.
(2) Low friction: lower frictional coefficients tend to destabilise the interface. This is because the tractional mismatch between normal and shear tractions is more easily resolved if the interface is highly effective in transferring shear tractions across, which happens with higher frictional coefficients.
(3) Similarly, small normal loads (or large shear loads).

Once the detachment has taken place, the contact conditions are violated and the interface detaches, rendering the contact formulation aimed at determining the zones of stick and slip invalid. Beyond its initiation, the analytical modelling of the interfacial detachment process appears extremely challenging owing to its non-linearity: once detachment occurs, it does so only locally, and part of the interface remains attached whereas another part detaches; likewise, it is possible for contact to be re-established at least partially, particularly if the remote normal loads are considerable. This makes the explicit computation of the detailed detachment–reattachment problem highly challenging and, owing to the inherent ill-posedness of such problems (Simoes and Martins, 1998), difficult to achieve even numerically.

7. Conclusions

This article has examined the problem of planar bimaterial frictional contact under transient loads. Explicit solutions to the transient loads caused by remote normal and shear loads have been derived, as well as for the slip wave that may be triggered under bimaterial contact. It has been shown that uncoupled contact, i.e., contact where it is possible to neglect the vertical displacement of the interface, is an unacceptable approximation under bimaterial conditions. This was because the interface unable to sustain uncoupled slip waves without causing the two faces in contact to either interpenetrate one another,

or to detach: either situation is in direct violation of Coulomb's laws of contact, and as result it was concluded that transient uncoupled slip is impossible when the two materials across an elastic interface are different. Furthermore, it has been argued that even as an approximation, the uncoupled problem appears inconsistent: the vertical displacements are of the same order of magnitude as the interfacial slip. The only way for the uncoupled problem to remain an acceptable approximation is for the two materials in contact to have the same elastic constants, which reverts the problem to the far more tractable one of single material contact.

It has been shown that the only way to model the bimaterial contact under transient loading is to explicitly model the coupling between shear and normal loads at the interface. This was achieved by superposing the uncoupled problem with a set of corrective normal and shear tractions defined so as to enforce that the contact interface remains vertically compatible during the loading and, as a result, fully coupled. These two new corrective tractions have been derived by solving a fully coupled inhomogeneous Wiener–Hopf matricial problem. Owing to the branch cuts in the scattering kernels in the ensuing Riemann–Hilbert problem, it was not possible to attain a product decomposition of the scattering kernel matrix in the resulting Wiener–Hopf problem. However, using an Abrahams approach reliant on the approximation of the irreducible terms with their Padé approximant, it has been shown it is possible to achieve a coupled, approximate solution that retains the near and far field character of the solution even for the lowest order approximation, and that it is quickly convergent to the exact solution as the order of the Padé approximant is increased. Thus, the coupled contact problem has been solved using an infinite regression of the scattering kernel.

A series of features were observed in the solution of the coupled bimaterial frictional contact problem. First, the role of the Stoneley waves was revealed to lead to a regime of reverse slip in the spatial region lying between the head wave and the first Stoneley wave. This reversal entails a change in the sign of the interface shear and, as a result, is expected to have negative consequences for the wear performance of the interface, as well as being a source of vibrations in the far field if the bimaterial interface occurs in geological materials. Second, the possibility of interfacial detachment was examined. For this, an explicit, closed-form function was developed with which to assess the stability of the bimaterial interface under different loading, frictional coefficients, and materials constants. The function was used to explore the stability of the interface across a broad range of parameters, the general findings of which were that, *caeteris paribus*, lower friction coefficients and increasing disparity in the elastic contacts of the two materials in contact tend to destabilise the latter and promote detachment across the interface.

The approach allows us to gain a physical insight as for the reasons behind said detachment: it is caused by the mismatch between the shear and normal tractions the remote loads induce across the interface. These tractions are transmitted by a four-wavefront structure (two longitudinal and two transverse wavefronts), which can be such that the interface, in attempting to accommodate a normal load by promoting slip, may at the same time cause the normal traction to change sign, thereby violating the contact conditions at the interface, which tends to detach as a result. As was argued, although the interfacial instability can be modelled and is inherent to the material conditions of the contact, the subsequent process of detachment and re-attachment is so highly non-linear that it appears difficult to model it through an explicit analytical treatment. Nevertheless, the criterion developed here can be employed as a simple rule of thumb with which to assess the likelihood of the detachment in transient contact, and offers an useful pathway for ensuring, through lubrication strategies or interfacial design, that detachment does not take place, and if it does, to model the far field signals by means of deducing the interfacial tractions that caused them. Generally speaking, the best remedy against detachment appears to be to increase the intensity of the remote contact pressure.

Thus, this work has for the first time provided (1) a fully analytical treatment of the coupled bimaterial interface, including interfacial tractions and contact conditions, which enables the explicit, analytic modelling of stress wave scattering at contact interfaces; (2) an exact criterion for establishing the transient stability of a bimaterial contact interface subject to dry friction. It is expected that the analytical treatment of the transient loads offered here will be used to study in detail specific contact interfaces and produce detachment and slip envelops based on the. This will pave the way towards a better understanding of the delamination process in composite materials, and an accurate modelling of the seismological signals brought about by fault surface separation in dissimilar layers in shallow Earth.

Declaration of competing interest

The authors declare that they have no known competing financial interests or personal relationships that could have appeared to influence the work reported in this paper.

Data availability

No data was used for the research described in the article

Acknowledgements

The author conceived and wrote the whole article.

Appendix A

The mathematical expression for the $K_+(k)$ and $G_+(k)$ kernels for the non-vanishing interfacial tractions of, respectively, a mode I and mode II crack are the following:

$$K_+(k) = S_2^+(k)F_+(k), \tag{A.1}$$

$$G_+(k) = -S_2^+(k)H_+(k) \tag{A.2}$$

where

$$S_2^+(k) = \frac{\alpha_2^+(k)}{(c_2+k)D_2^+(k)}\sqrt{\frac{b_2^2}{2(a_2^2-b_2^2)\mu_2}} \tag{A.3}$$

with

$$\alpha_2^+(k) = \sqrt{a_2+k} \tag{A.4}$$

$$\ln D_2^+(k) = -\frac{1}{\pi}\int_{a_2}^{b_2} \arctan\left[\frac{4z^2\sqrt{z^2-a_2^2}\sqrt{b_2^2-z^2}}{(b_2^2-2z^2)^2}\right]\frac{\mathrm{d}z}{z+k} \tag{A.5}$$

The two subkernels $F_+(k)$ and $H_+(k)$ are

$$\ln F_+(k) = \mp\left\{\frac{1}{\pi}\left[\int_{a_1}^{a_2} f_a(z)\frac{\mathrm{d}z}{z+k} + \int_{a_2}^{b_1} f_b(z)\frac{\mathrm{d}z}{z+k} + \int_{b_1}^{b_2} f_c(z)\frac{\mathrm{d}z}{z+k}\right] + \ln\kappa\right\} \tag{A.6}$$

$$\ln H_+(k) = \mp\left\{\frac{1}{\pi}\left[\int_{a_1}^{a_2} h_a(z)\frac{\mathrm{d}z}{z+k} + \int_{a_2}^{b_1} h_b(z)\frac{\mathrm{d}z}{z+k} + \int_{b_1}^{b_2} h_c(z)\frac{\mathrm{d}z}{z+k}\right] + \ln\eta\right\} \tag{A.7}$$

Here κ and η are constants:

$$\kappa = 1 + \frac{\mu_2 b_1^2(a_2^2-b_2^2)}{\mu_1 b_2^2(a_1^2-b_1^2)} \tag{A.8}$$

$$f_a(k) = \arctan\left[\frac{4k^2\bar{B}_1(k)\left(b_1^2\mu_2\left(k^2-a_1^2\right)\left(4k^2\sqrt{a_2^2-k^2}\bar{B}_2(k)+\left(b_2^2-2k^2\right)^2\right)+b_2^2\mu_1A_1(k)\sqrt{a_2^2-k^2}\right)}{\left(b_1^2-2k^2\right)^2\left(b_1^2\mu_2A_1(k)\left(4k^2\sqrt{a_2^2-k^2}\bar{B}_2(k)+\left(b_2^2-2k^2\right)^2\right)-b_2^2\mu_1\sqrt{a_2^2-k^2}\right)}\right] \tag{A.10}$$

Box I.

$$f_c^{(1)}(k) = \frac{-b_1^2\mu_2A_2(k)\left(-4k^2A_1(k)B_1(k)+b_1^4-4b_1^2k^2+4k^4\right)-b_2^6\mu_1A_1(k)+4b_2^4k^2\mu_1A_1(k)-4b_2^2k^4\mu_1A_1(k)}{4b_2^2k^2\mu_1A_1(k)A_2(k)\bar{B}_2(k)} \tag{A.15}$$

Box II.

$$\eta = 1+\frac{b_1^2\mu_2\left(a_2^2-b_2^2\right)}{b_2^2\mu_1\left(a_1^2-b_1^2\right)}, \tag{A.9}$$

and $f_i(k)$ and $h_i(k)$ are influence functions given by (see Box I).

$$f_b(k) = \arctan\left[\frac{f_b^{(1)}}{f_b^{(2)}}\right] \tag{A.11}$$

with

$$\begin{aligned}
f_b^{(1)} &= b_1^4\left(-16k^4\mu_2\left(a_1^2+k^2\right)A_2(k)+b_2^6\mu_1A_1(k)\right.\\
&\left.-4b_2^4k^2\mu_1A_1(k)+4b_2^2k^4\mu_1A_1(k)\right)-\\
&-4b_1^2\left(-4a_1^2k^6\mu_2A_2(k)+b_2^6k^2\mu_1A_1(k)-4b_2^4k^4\mu_1A_1(k)+4b_2^2k^6\mu_1A_1(k)\right)+\\
&+4b_2^2k^4\mu_1\left(-4a_1^2A_2(k)\bar{B}_1(k)\bar{B}_2(k)+b_2^4A_1(k)-4b_2^2k^2A_1(k)+4k^4A_1(k)+\right.\\
&\left.+4k^2A_2(k)\bar{B}_1(k)\bar{B}_2(k)\right)+b_1^{10}\mu_2A_2(k)\\
&-8b_1^8k^2\mu_2A_2(k)+24b_1^6k^4\mu_2A_2(k)
\end{aligned} \tag{A.12}$$

$$\begin{aligned}
f_b^{(2)} &= 4b_2^2k^2\mu_1\left(-b_1^4A_1(k)A_2(k)\bar{B}_2(k)+k^2\left(4b_1^2A_1(k)A_2(k)\bar{B}_2(k)-\right.\right.\\
&-\left.4k^2A_1(k)A_2(k)\bar{B}_2(k)+b_2^4\bar{B}_1(k)-4b_2^2k^2\bar{B}_1(k)+4k^4\bar{B}_1(k)\right)\\
&\left.-a_1^2\bar{B}_1(k)\left(b_2^2-2k^2\right)^2\right)
\end{aligned} \tag{A.13}$$

$$f_c(k) = \arctan\left[f_c^{(1)}(k)\right] \tag{A.14}$$

with $A_i(k)=\sqrt{k^2-a_i^2}$, $B_i(k)=\sqrt{k^2-b_i^2}$, $\bar{B}_i(k)=\sqrt{b_i^2-k^2}$ (see Box II).

$$h_a(k) = \arctan\left[\frac{h_a^{(1)}}{h_a^{(2)}}\right], h_b(k) = \arctan\left[\frac{h_b^{(1)}}{h_b^{(2)}}\right] \tag{A.16}$$

$$\begin{aligned}
h_a^{(1)} &= 16b_2^2k^4\mu_1\left(k^2-a_1^2\right)\left(b_1^2-k^2\right)\bar{B}_2(k)+\mu_2\left(b_1^3-2b_1k^2\right)^2\\
&\bar{B}_1(k)\left(4k^2\sqrt{a_2^2-k^2}\bar{B}_2(k)+\left(b_2^2-2k^2\right)^2\right)+\\
&+\left(b_1^2-2k^2\right)^4
\end{aligned}$$

and

$$h_a^{(2)} = 4b_1^2k^2\mu_2A_1(k)\left(b_1^2-k^2\right)\left(4k^2\sqrt{a_2^2-k^2}\bar{B}_2(k)+\left(b_2^2-2k^2\right)^2\right), \tag{A.17}$$

$$\begin{aligned}
h_b^{(1)} &= 4b_1^2k^4\left(4k^2\mu_2\left(A_1(k)A_2(k)\bar{B}_2(k)-k^2\bar{B}_1(k)\right)+4a_1^2b_2^2\mu_1\bar{B}_2(k)-b_2^4\mu_2\bar{B}_1(k)\right.\\
&\left.+4b_2^2k^2\left(\mu_2\bar{B}_1(k)+\mu_1\bar{B}_2(k)\right)\right)-4b_1^4\left(4k^4\mu_2\left(A_1(k)A_2(k)\bar{B}_2(k)-k^2\bar{B}_1(k)\right)-\right.\\
&\left.-b_2^4k^2\mu_2\bar{B}_1(k)+2b_2^2k^4\left(2\mu_2\bar{B}_1(k)+3\mu_1\bar{B}_2(k)\right)\right)\\
&-16a_1^2b_2^2k^6\mu_1\bar{B}_2(k)-b_1^8b_2^2\mu_1\bar{B}_2(k)+\\
&+b_1^6\left(-b_2^4\mu_2\bar{B}_1(k)+4b_2^2k^2\left(\mu_2\bar{B}_1(k)+2\mu_1\bar{B}_2(k)\right)-4k^4\mu_2\bar{B}_1(k)\right)
\end{aligned}$$

$$\begin{aligned}
h_b^{(2)} &= 4b_1^2k^2\mu_2\left(-b_1^2\left(b_2^4A_1(k)-4b_2^2k^2A_1(k)+4k^4A_1(k)+4k^2A_2(k)\bar{B}_1(k)\bar{B}_2(k)\right)+\right.\\
&\left.+b_2^4k^2A_1(k)-4b_2^2k^4A_1(k)+4k^6A_1(k)+4k^4A_2(k)\bar{B}_1(k)\bar{B}_2(k)+b_1^4A_2(k)\bar{B}_1(k)\bar{B}_2(k)\right),
\end{aligned}$$

and finally (see Box III)

Appendix B

The mathematical form of $\frac{\partial^2}{\partial t^2}\mathrm{Im}\left[\frac{1}{J\left(-\frac{t-t_0}{x-x_0}\right)}\right]$

$$\frac{\partial^2}{\partial t^2}\mathrm{Im}\left[\frac{1}{J\left(-\frac{t-t_0}{x-x_0}\right)}\right] = \frac{1}{x^2}\mathrm{Im}\left[\frac{A(u)}{B(u)}\right]$$

where $u=-\frac{t-t_0}{x-x_0}$ and

$$B(u) = \left(b_1^2\beta_1(u)\mu_2R_2(u)+b_2^2\beta_2(u)\mu_1R_1(u)\right)^3$$

$$\begin{aligned}
\frac{1}{\mu_1\mu_2}A(u) &= b_1^2\mu_2\beta_1R_2^2\left(b_1^2\mu_2R_2\left(2\beta_1'R_1'-\beta_1R_1''\right)+2b_2^2\mu_1\beta_2(R_1')^2\right)-\\
&-b_1^2\mu_2R_1R_2\left(b_1^2\mu_2R_2^2\left(2(\beta_1')^2-\beta_1\beta_1''\right)+b_2^2\mu_1R_2\left(2\beta_2\beta_1'R_1'-4\beta_1\beta_2'R_1'+\beta_1\beta_2R_1''\right)\right.\\
&\left.+4b_2^2\mu_1\beta_1\beta_2R_1'R_2'\right)+\\
&+b_1^2b_2^2\mu_1\mu_2R_1^2\left(R_2\left(4\beta_2\beta_1'R_2'-2\beta_1\beta_2'R_2'-\beta_1\beta_2R_2''\right)+R_2^2\left(\beta_2\beta_1''-4\beta_1'\beta_2'+\beta_1\beta_2''\right)\right.\\
&\left.+2\beta_1\beta_2(R_2')^2\right)+\\
&+b_2^4\mu_1^2R_1^3\left(\beta_2\left(2\beta_2'R_2'-\beta_2R_2''\right)+R_2\left(\beta_2\beta_2''-2(\beta_2')^2\right)\right)
\end{aligned}$$

with

$$\begin{aligned}
\alpha_n(u) &= \sqrt{a_n^2-u^2}\\
\alpha_n'(u) &= -\frac{u}{\sqrt{a_n^2-u^2}}\\
\alpha_n''(u) &= -\frac{a_n^2}{(a_n^2-u^2)^{3/2}}\\
\beta_n(u) &= \sqrt{b_n^2-u^2}\\
\beta_n'(u) &= -\frac{u}{\sqrt{b_n^2-u^2}}\\
\beta_n''(u) &= -\frac{b_n^2}{(b_n^2-u^2)^{3/2}}\\
R_n(u) &= (b_n^2-2u^2)^2+4u^2\alpha_n\beta_n
\end{aligned}$$

$$h_c(k) = \arctan\left[-\frac{\bar{B}_2(k)\left(4b_2^2k^2\mu_1\left(k^2 - A_1(k)B_1(k)\right) - 4b_1^2k^2\left(\mu_2A_2(k)B_1(k) + b_2^2\mu_1\right) + b_1^4b_2^2\mu_1\right)}{b_1^2\mu_2B_1(k)\left(b_2^2 - 2k^2\right)^2}\right] \tag{A.18}$$

Box III.

$$\begin{aligned}
R_n'(u) &= -8u(b_n^2 - 2u^2) + 8u\alpha_n\beta_n + 4u^2\alpha_n'\beta_n + \\
&\quad + 4u^2\alpha_n\beta_n' \\
R_n''(u) &= -8(b_n^2 - 6u^2) + 8\alpha_n\beta_n + 16u\alpha_n'\beta_n + \\
&\quad + 16u\alpha_n\beta_n' + 4u^2\alpha_n''\beta_n + \\
&\quad + 4u^2\alpha_n\beta_n'' + 8u^2\alpha_n'\beta_n'
\end{aligned}$$

Appendix C

A numerical procedure to solve Eq. (5.56) is outlined here. Crucially, all terms in the equation can be expressed in terms of $k = t/x$, it is possible to employ a one dimensional Nyström collocation method to solve it numerically. The problem can be expressed as

$$\begin{aligned}
&\langle F(k) + Q^*(k) - f\,\mathrm{sign}(f)P^*(k), \ddot{\phi}(k)\rangle \\
&= f\,\mathrm{sign}(f)P(k) - Q(k)
\end{aligned} \tag{C.19}$$

where $F(k)$ is the kernels described above. We seek $\ddot{\phi}(k)$, the distribution of slip velocities.

We find it numerically by discretising the solution domain $k \in [0, \infty]$ into N subintervals and $N + 1$ collocation points. The form of the distribution of slip is approximated by a Galerkin function

$$\ddot{\phi}(k) = \sum_{i=1}^{n} \phi_i N_i(k) \tag{C.20}$$

where ϕ_i is the nodal value, and $N_i(k)$ are some basis functions. We choose $N_i(k)$ to linearly interpolate the node i with value 1 and take value 0 in all other nodes. The solution we seek is the n nodal values ϕ_i, for which we need n equations. We have:

$$\begin{aligned}
&\sum_{i=1}^{n} v_i\langle F(k) + Q^*(k) - f\,\mathrm{sign}(f)P^*(k), N_i(k)\rangle = \\
&= f\,\mathrm{sign}(f)P(k) - Q(k)
\end{aligned} \tag{C.21}$$

We can obtain the n equations by *collocating* n k-points along the real line. If $\{k_i\}$ represents the n nodes and k_j the n collocation nodes, we can rewrite the system of equations as:

$$F_{ji}^{\mathrm{tot}}\phi_i = f\,\mathrm{sign}(f)p_j - q_j \tag{C.22}$$

where $f_j \equiv f(k_j)$ and $f_i =\equiv f(k_i)$. The values of p_j and q_j can be directly evaluated. Those of F_{ji}^{tot} come from evaluating:

$$F_{ji}^{\mathrm{tot}} = \langle F(k) + Q^*(k) - f\,\mathrm{sign}(f)P^*(k), N_i(k)\rangle\big|_{k=k_j}$$

Given that the support of each $N_i(k)$ is $k \in [k_{i-1}, k_{i+1}]$, most $F_{ji}^{\mathrm{tot}} = 0$ and the matrix is banded. The resulting problem is inherently ill-posed, and needs to be regularised. The solution ϕ_i can be regularised using a Tikhonov regularisation scheme with $\Gamma_{ji} = \lambda\delta_{ji}$ the Tikhonov matrix for λ the regularisation parameter to be adjusted. This leads to a regularised solution:

$$\hat{\phi}_i = (F_{ij}^{\mathrm{tot}}F_{ji}^{\mathrm{tot}} + \Gamma_{ji}\Gamma_{ij})^{-1}F_{ji}^{\mathrm{tot}}(f\,\mathrm{sign}(f)p_j - q_j)$$

References

Abascal, R., 1995. 2D transient dynamic friction contact problems. I. Numerical analysis. Eng. Anal. Bound. Elem. 16 (3), 227–233.

Abedi, R., Haber, R.B., 2014. Riemann solutions and spacetime discontinuous galerkin method for linear elastodynamic contact. Comput. Methods Appl. Mech. Engrg. 270, 150–177.

Abrahams, I.D., 1996. Radiation and scattering of waves on an elastic half-space; a non-commutative matrix Wiener-Hopf problem. J. Mech. Phys. Solids 44 (12), 2125–2154.

Abrahams, I.D., 2000. The application of Padé approximants to Wiener–Hopf factorization. IMA J. Appl. Math. 65 (3), 257–281.

Abrahams, I.D., 2002. On the application of the Wiener-Hopf technique to problems in dynamic elasticity. Wave Motion 36 (4), 311–333.

Achenbach, J.D., 1973. Wave Propagation in Elastic Solids. North-Holland, New York.

Achenbach, J.D., Bažant, Z.P., Khetan, R.P., 1976. Elastodynamic near-tip fields for a rapidly propagating interface crack. Internat. J. Engrg. Sci. 14 (9), 797–809.

Adams, G.G., 1995. Self-excited oscillations of two elastic half-spaces sliding with a constant coefficient of friction. J. Appl. Mech. 62 (4), 867–872.

Adams, G.G., 1998. Dynamic instabilities in the sliding of two layered elastic half-spaces. J. Tribol. 120 (2), 289–295.

Aki, K., Richards, P.G., 2002. Quantitative Seismology, second ed. University Science Books, Sausalito, CA.

Andrews, E.H., Kinloch, A.J., 1973. Mechanics of adhesive failure. II. Proc. Phys. Soc. A 332 (1590), 401–414.

Atkinson, C., 1974. On the dynamic stress and displacement field associated with a crack propagating across the interface between two media. Internat. J. Engrg. Sci. 12 (6), 491–506.

Baik, J.-M., Thompson, R.B., 1984. Ultrasonic scattering from imperfect interfaces: a quasi-static model. J. Nondestruct. Eval. 4 (3), 177–196.

Baker, G.A., Graves Morris, P., 1996. Padé Approximants, second ed. In: Encyclopedia of Mathematics and Its Applications, Cambridge University Press.

Barber, J.R., 2018. Contact Mechanics. Springer, Cham, CH.

Blanloeuil, P., Croxford, A.J., Meziane, A., 2014. Numerical and experimental study of the nonlinear interaction between a shear wave and a frictional interface. J. Acoust. Soc. Am. 135 (4), 1709–1716.

Blanloeuil, P., Rose, L.R.F., Veidt, M., Wang, C.H., 2019. Analytical and numerical modelling of wave scattering by a linear and nonlinear contact interface. J. Sound Vib. 456, 431–453.

Blanpied, M.L., Lockner, D.A., Byerlee, J.D., 1995. Frictional slip of granite at hydrothermal conditions. J. Geophys. Res.: Solid Earth 100 (B7), 13045–13064.

Broberg, K.B., 1999. Cracks and Fracture. Academic Press, London.

Brock, L.M., 2002. Exact analysis of dynamic sliding indentation at any constant speed on an orthotropic or transversely isotropic half-space. J. Appl. Mech. 69 (3), 340–345.

Brock, L.M., 2012. Two cases of rapid contact on an elastic half-space: sliding ellipsoidal die, rolling sphere. J. Mech. Mater. Struct. 7 (5), 469–483.

Cagniard, L., 1939. Réflexion et Réfraction Des Ondes Séismique Progressives. Gauthiers-Villars, Paris.

Cao, H.C., Evans, A.G., 1989. An experimental study of the fracture resistance of bimaterial interfaces. Mech. Mater. 7 (4), 295–304.

Carlson, J.M., Langer, J.S., 1989. Mechanical model of an earthquake fault. Phys. Rev. A 40 (11), 6470.

Cattaneo, C., 1938. Sul contatto di due corpi elastici: distribuzione locale degli sforzi. Rc. Accad. Naz. Lincei 27 (342–348, 434–436, 474–478).

Chez, E.L., Dundurs, J., Comninou, M., 1978. Reflection and refraction of sh waves in presence of slip and friction. Bull. Seismol. Soc. Am. 68 (4), 999–1011.

Clancey, K.F., Gohberg, I., 2013. Factorization of Matrix Functions and Singular Integral Operators. Vol. 3, Birkhäuser.

Comninou, M., 1977. Interface crack with friction in the contact zone. J. Appl. Mech. 44, 780–781.

Comninou, M., 1984. Interface disturbances caused by plane elastic pulses. Internat. J. Engrg. Sci. 22 (8–10), 1135–1138.

Comninou, M., Achenbach, J.D., 1978. Asymptotic fields at the transition zone of a propagating interface crack. Mech. Res. Commun. 5 (5), 285–290.

Comninou, M., Dundurs, J., 1977. Elastic interface waves involving separation. J. Appl. Mech. 44 (2), 222–226.

Craggs, J.W., Roberts, A.M., 1967. On the motion of a heavy cylinder over the surface of an elastic solid. J. Appl. Mech. 34 (1), 207–209.

De Hoop, A.T., 1960. A modification of Cagniard's method for solving seismic pulse problems. Appl. Sci. Res. B 8, 349–356.

Delsanto, P.P., Scalerandi, M., 1998. A spring model for the simulation of the propagation of ultrasonic pulses through imperfect contact interfaces. J. Acoust. Soc. Am. 104 (5), 2584–2591.

Dini, D., Hills, D.A., 2003. A method based on asymptotics for the refined solution of almost complete partial slip contact problems. Eur. J. Mech. A Solids 22 (6), 851–859.

Dini, D., Hills, D.A., 2004. Bounded asymptotic solutions for incomplete contacts in partial slip. Int. J. Solids Struct. 41 (24–25), 7049–7062.
Eringen, A.C., Suhubi, E.S., 1975. Elastodynamics. Vol. 2, Academic Press, New York.
Eshelby, J.D., 1956. Supersonic dislocations and dislocations in dispersive media. Proc. Phys. Soc. 69 (10), 1013–1019.
Fregly, B.J., Bei, Y., Sylvester, M.E., 2003. Experimental evaluation of an elastic foundation model to predict contact pressures in knee replacements. J. Biomech. 36 (11), 1659–1668.
Freund, L.B., 1972. Energy flux into the tip of an extending crack in an elastic solid. J. Elasticity 2 (4), 341–349.
Gao, Y.C., Shi, Z.F., 1994. Large strain field near an interface crack tip. Int. J. Fract. 69 (3), 269–279.
Georgiadis, H.G., Barber, J.R., 1993. On the super-rayleigh/subseismic elastodynamic indentation problem. J. Elasticity 31 (3), 141–161.
Georgiadis, H.G., Charalambakis, N., 1994. An analytical/numerical approach for cracked elastic strips under concentrated loads—transient response. Int. J. Fract. 65 (1), 49–61.
Geubelle, P.H., Knauss, W.G., 1994a. Finite strains at the tip of a crack in a sheet of hyperelastic material: I. Homogeneous case. J. Elasticity 35 (1–3), 61–98.
Geubelle, P.H., Knauss, W.G., 1994b. Finite strains at the tip of a crack in a sheet of hyperelastic material: II. Special bimaterial cases. J. Elasticity 35 (1–3), 99–137.
Geubelle, P.H., Knauss, W.G., 1994c. Finite strains at the tip of a crack in a sheet of hyperelastic material: III. General bimaterial case. J. Elasticity 35 (1–3), 139–174.
Golub, M.V., Doroshenko, O.V., 2019. Boundary integral equation method for simulation scattering of elastic waves obliquely incident to a doubly periodic array of interface delaminations. J. Comput. Phys. 376, 675–693.
Gurrutxaga-Lerma, B., 2019. On the transient dynamic antiplane contact problem in the presence of dry friction and slip. Int. J. Solids Struct. 170, 142–156.
Gurrutxaga-Lerma, B., 2020. On the transient planar contact problem in the presence of dry friction and slip. Int. J. Solids Struct. 193, 314–327.
Gurrutxaga-Lerma, B., 2021. The elastodynamic bimaterial interface under mode I and mode II loading. Int. J. Solids Struct. 225, 111031.
Gurrutxaga-Lerma, B., Verschueren, J., Sutton, A.P., Dini, D., 2020. The mechanics and physics of high-speed dislocations: a critical review. Int. Mater. Rev. 1–41.
Hao, S., Liu, W.K., Klein, P.A., Rosakis, A.J., 2004. Modeling and simulation of intersonic crack growth. Int. J. Solids Struct. 41 (7), 1773–1799.
Hassani-Gangaraj, M., Veysset, D., Nelson, K.A., Schuh, C.A., 2019. Impact-bonding with aluminum, silver, and gold microparticles: Toward understanding the role of native oxide layer. Appl. Surf. Sci. 476, 528–532.
Hériveaux, Y., Nguyen, V.-H., Haïat, G., 2018. Reflection of an ultrasonic wave on the bone-implant interface: A numerical study of the effect of the multiscale roughness. J. Acoust. Soc. Am. 144 (1), 488–499.
Hills, D.A., Kelly, P.A., Dai, D.N., Korsunsky, A.M., 1996. Solution of crack problems: the distributed dislocation technique. In: Volume 44 of Solid Mechanics and Its Applications. Kluwer Academic Publishers, Boston.
Huang, Y., Liu, C., Rosakis, A.J., 1996. Transonic crack growth along a bimaterial interface: an investigation of the asymptotic structure of near-tip fields. Int. J. Solids Struct. 33 (18), 2625–2645.
Hutchinson, J.W., Jensen, H.M., 1990. Models of fiber debonding and pullout in brittle composites with friction. Mech. Mater. 9 (2), 139–163.
Jhang, K.-Y., 2009. Nonlinear ultrasonic techniques for nondestructive assessment of micro damage in material: a review. Int. J. Precis. Eng. Manuf. 10 (1), 123–135.
Johnson, K.L., 1987. Contact Mechanics. Cambridge Univ. Press, Cambridge, UK.
Kilgore, B., Beeler, N.M., Lozos, J., Oglesby, D., 2017. Rock friction under variable normal stress. J. Geophys. Res.: Solid Earth 122 (9), 7042–7075.
Knowles, J.K., Sternberg, E., 1983. Large deformations near a tip of an interface-crack between two neo-hookean sheets. J. Elasticity 13 (3), 257–293.
Lambros, J., Rosakis, A.J., 1995. Shear dominated transonic interfacial crack growth in a bimaterial-I. Experimental observations. J. Mech. Phys. Solids 43 (2), 169–188.
Lapusta, N., Rice, J.R., Ben-Zion, Y., Zheng, G., 2000. Elastodynamic analysis for slow tectonic loading with spontaneous rupture episodes on faults with rate-and state-dependent friction. J. Geophys. Res.: Solid Earth 105 (B10), 23765–23789.
Lavrentyev, A.I., Rokhlin, S.I., 1998. Ultrasonic spectroscopy of imperfect contact interfaces between a layer and two solids. J. Acoust. Soc. Am. 103 (2), 657–664.
Leterrier, Y., 2003. Durability of nanosized oxygen-barrier coatings on polymers. Prog. Mater. Sci. 48 (1), 1–55.
Liu, C., Huang, Y., Rosakis, A.J., 1995. Shear dominated transonic interfacial crack growth in a bimaterial. II. asymptotic fields and favorable velocity regimes. J. Mech. Phys. Solids 43 (2), 189–206.
Liu, C., Lambros, J., Rosakis, A.J., 1993. Highly transient elastodynamic crack growth in a bimaterial interface: higher order asymptotic analysis and optical experiments. J. Mech. Phys. Solids 41 (12), 1887–1954.
Mantič, V., 2009. Interface crack onset at a circular cylindrical inclusion under a remote transverse tension, application of a coupled stress and energy criterion. Int. J. Solids Struct. 46 (6), 1287–1304.
Markushevich, A.I., 2005a. Theory of Functions of a Complex Variable, second ed. Vol. III, American Mathematical Society, Providence, RI.
Markushevich, A.I., 2005b. Theory of Functions of a Complex Variable, second ed. Vol. I, American Mathematical Society, Providence, RI.
McKinley, T.O., Rudert, M.J., Koos, D.C., Pedersen, D.R., Baer, T.E., Tochigi, Y., Brown, T.D., 2006. Contact stress transients during functional loading of ankle stepoff incongruities. J. Biomech. 39 (4), 617–626.
Minato, S., Ghose, R., 2014. Imaging and characterization of a subhorizontal non-welded interface from point source elastic scattering response. Geophys. J. Int. 197 (2), 1090–1095.
Needleman, A., Rosakis, A.J., 1999. The effect of bond strength and loading rate on the conditions governing the attainment of intersonic crack growth along interfaces. J. Mech. Phys. Solids 47 (12), 2411–2449.
Noble, B., 1958. Methods based on the Wiener–Hopf technique for the solution of partial differential equations. In: Volume 7 of International Series of Monographs on Pure and Applied Mathematics. Pergamon Press, New York.
Nowell, D., Hills, D.A., Sackfield, A., 1988. Contact of dissimilar elastic cylinders under normal and tangential loading. J. Mech. Phys. Solids 36 (1), 59–75.
Olami, Z., Feder, Hans J.S., Christensen, K., 1992. Self-organized criticality in a continuous, nonconservative cellular automaton modeling earthquakes. Phys. Rev. Lett. 68 (8), 1244.
Rice, J.R., 1988. Elastic fracture mechanics concepts for interfacial cracks. J. Appl. Mech. 55 (1), 98–103.
Rice, J.R., 1993. Spatio-temporal complexity of slip on a fault. J. Geophys. Res.: Solid Earth 98 (B6), 9885–9907.
Rice, J.R., Lapusta, N., Ranjith, K., 2001. Rate and state dependent friction and the stability of sliding between elastically deformable solids. J. Mech. Phys. Solids 49 (9), 1865–1898.
Rice, J.R., Ruina, A.L., 1983. Stability of steady frictional slipping. J. Appl. Mech. 50 (2), 343–349.
Rosakis, A.J., Samudrala, O., Singh, R.P., Shukla, A., 1998. Intersonic crack propagation in bimaterial systems. J. Mech. Phys. Solids 46 (10), 1789–1814.
Scala, A., Festa, G., Villote, J.P., 2017. Rupture dynamics along bimaterial interfaces: a parametric study of the shear-normal traction coupling. Geophys. J. Int. 209 (1), 48–67.
Schallamach, A., 1971. How does rubber slide? Wear 17 (4), 301–312.
Scholte, J.G., 1947. The range of existence of Rayleigh and stoneley waves. In: Geophysical Supplements to the Monthly Notices of the Royal Astronomical Society. Vol. 5, (5), pp. 120–126.
Scholz, C.H., 1998. Earthquakes and friction laws. Nature 391 (6662), 37.
Scholz, C.H., 2019. The Mechanics of Earthquakes and Faulting. Cambridge Univ. Press.
Simoes, F.M.F., Martins, J.A.C., 1998. Instability and ill-posedness in some friction problems. Internat. J. Engrg. Sci. 36 (11), 1265–1293.
Sinclair, G.B., 2004a. Stress singularities in classical elasticity–I: Removal, interpretation, and analysis. Appl. Mech. Rev. 57 (4), 251–297.
Sinclair, G.B., 2004b. Stress singularities in classical elasticity–II: Asymptotic identification. Appl. Mech. Rev. 57 (5), 385–439.
Slepyan, L.I., Brun, M., 2012. Driving forces in moving-contact problems of dynamic elasticity: Indentation, wedging and free sliding. J. Mech. Phys. Solids 60 (11), 1883–1906.
Stallard, J., Poulat, S., Teer, D.G., 2006. The study of the adhesion of a tin coating on steel and titanium alloy substrates using a multi-mode scratch tester. Tribol. Int. 39 (2), 159–166.
Tiamiyu, A.A., Chen, X., Pang, E.L., Sun, Y., Lienhard, J., LeBeau, J.M., Nelson, K.A., Schuh, C.A., 2022. Oxide layer delamination: An energy dissipation mechanism during high-velocity microparticle impacts. Appl. Surf. Sci. 574, 151673.
Weertman, J., 1980. Unstable slippage across a fault that separates elastic media of different elastic constants. J. Geophys. Res.: Solid Earth 85 (B3), 1455–1461.
Williams, M.L., 1959. The stresses around a fault or crack in dissimilar media. Bull. Seismol. Soc. Am. 49 (2), 199–204.
Xu, X.-P., Needleman, A., 1996. Numerical simulations of dynamic crack growth along an interface. Int. J. Fract. 74 (4), 289–324.
Yang, W., Suo, Z., Shih, C.F., 1991. Mechanics of dynamic debonding. Proc. R. Soc. Lond. Ser. A 433 (1889), 679–697.
Yu, G.-L., Wang, Y.-S., Li, G.-S., 2006. Frictional slip of an elastic layer on a half-space caused by an anti-plane wave of an arbitrary form. J. Sound Vib. 294 (1–2), 238–248.
Yu, H., Yang, W., 1995. Mechanics of transonic debonding of a bimaterial interface: The in-plane case. J. Mech. Phys. Solids 43 (2), 207–232.